Analytical Methods

Accepted Manuscript

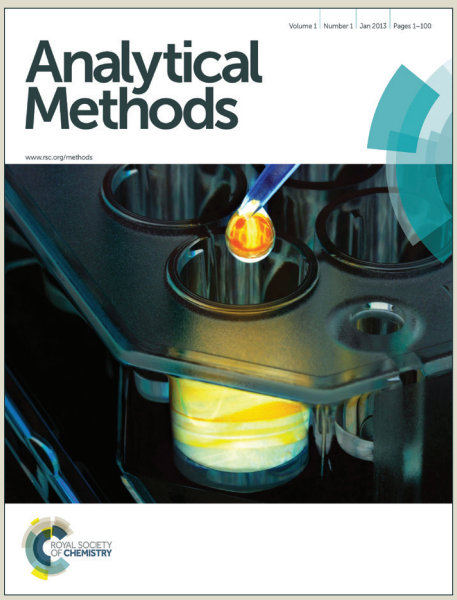

ROYAL SOCIETY OF CHEMISTRY

www.rsc.org/methods

Cite this: DOI: 10.1039/c0xx00000x

www.rsc.org/xxxxxx

ARTICLE TYPE

1,8-Naphthyridinic fluorescent 'turn-on' and 'turn-off' chemosensors for detecting of F^- and Hg^{2+} ions mimicking INHIBIT molecular logic behaviour

Mandeep K. Chahal and Muniappan Sankar*

Received (in XXX, XXX) Xth XXXXXXXXX 20XX, Accepted Xth XXXXXXXXX 20XX
DOI: 10.1039/b000000x

Two new receptors viz. 2-bromoacetamido-5,7-dimethyl-1,8-naphthyridine (**1a**) and 2-chloroacetamido-5,7-dimethyl-1,8-naphthyridine (**1b**) containing 1,8-naphthyridine as fluorophore unit have been designed and synthesised. These receptors exhibited very high selectivity for F^- ions among the various tested anions such as $H_2PO_4^-$, OAc^-, Cl^-, Br^-, I^-, HSO_4^-, PF_6^-, ClO_4^-, BF_4^- and NO_3^- owing to anion-induced deprotonation of amide NH by F^- ion. Among the various tested cations (Na^+, Ag^+, Co^{2+}, Ni^{2+}, Cu^{2+}, Zn^{2+}, Cd^{2+}, Hg^{2+}, Pb^{2+} and Mn^{3+}), **1a** exhibited selective detection of Hg^{2+} ion by binding with N1 and N8 atoms of naphthyridine moiety. The receptor **1a** has been explored as dual-ion detector for F^- and Hg^{2+} ions in two contrasting modes (fluorescence 'turn-on' and 'turn-off') which is supported by spectroscopic and lifetime measurements. **1a** exhibited lower detection limits for F^- (0.4 ppm) and Hg^{2+} (2.4 ppm) ions. These receptors were recovered from anionic species of **1a** formed after addition F^- ions by treating with protic solvents such as CH_3OH. The mode of binding was also confirmed by spectroscopic and DFT studies. The chemical inputs of F^- and Hg^{2+} ions generate an output which satisfies the condition of two-input INHIBIT logic operator.

Introduction

The development of small molecule based sensors has been an attractive area of research over the past 25 years.[1] Current scientific research mainly focuses on betterment of human life and prevention of diseases in humans. In this regard, scientists across the globe are trying to explore different chemosensors that are capable of detecting various anions[1,2] and metal ions[3] which are harmful to the human body with regard to biological, physical, environmental and chemical implications.[1-3] Among the assortment of ions known to us, mercury and fluoride ions demand a special attention due to their infamous history. Among common anions, fluoride ion is undoubtedly important owing to its established role in dental care[4a] and clinical treatment for osteoporosis.[4b,4c] Overexposure to fluoride, on the other hand, can lead to acute gastric, fluorosis and kidney problems.[4d] Many examples of fluorescent receptors containing hydrogen bonding donor motif, lewis acidic sites, electron-deficient organic π-systems, etc. for fluoride ion sensing are known.[1a,2,5] Excess of mercury intake results in skin decolouring, desquamation and peripheral neuropathy and kidney failure, as it can easily pass through the biological membranes. The most famous of the incidents caused by mercury poisoning was the Minamata disease which resulted in the death of several thousands of people including infants and children in Japan.[6] A vast variety of chromogenic and/or fluorogenic sensors are reported for the detection of mercuric ions.[7] The fluorescent chemosensing technique takes precedence over other available procedures due to its high detection sensitivity, safety and simplicity which translates molecular recognition into tangible optical signals.[8] Any study, which converts a compound to a chemosensor is of high value because of their increasing demand for various measurement devices in the fields of life science and environmental science. The obtained luminescence output with appropriate molecular inputs can be further utilised in designing basic logical operations like OR, AND, NAND, INH etc.[9] Therefore, the design and construction of molecular systems capable of performing complex logic functions is of great scientific interest. Varied applications of fluorescent chemical sensors, in the detection of ions and integration of these ions towards the construction of multiple and complex Boolean operations, such as OR, AND, NAND, INH, NOR, XNOR, etc are of great interest for the construction of molecular scale computing.[10]

1,8-naphthyridine and its derivatives exhibit various types of biological activities,[11] have been widely used as guanine recognition reagents[12] and are utilised as bidentate ligands.[13] These receptors have been used for fluorometric recognition of various biologically significant substrates like carboxylic acids and polyphosphates through multi-hydrogen bonding

interactions.[14] However, there are only few reports on naphthyridine-based fluorescent probes for the detection of metal ions.[15] To the best of our knowledge, 1,8-naphthyridine derivatives have not been utilized for the detection of environmentally and biologically important anionic species such as F^- ions based on ''binding site-signalling subunit'' protocol till date. Also, the number of naphthyridine-based chemosensors for environmentally toxic Hg(II) ions[16] are limited to a few only.

Herein, we present the first 1,8-naphthyridine-based receptor for the dual-channel detection of environmentally and biologically important F^- and Hg^{2+} ions. To conclusively prove the experimental work, computational studies[17] were also carried out using Gaussian 09. The compound behaves as an INHIBIT logic gate with YES and NOT logic functions in the presence of F^- and Hg^{2+} as chemical inputs.

Results and discussion

2-Amino-5,7-dimethyl-1,8-naphthyridine (**2**)[18] upon stirring with haloacetyl halide in dry CH_2Cl_2 at RT gave receptors **1a** and **1b** (Scheme 1). The receptors were characterized by analytical and spectral techniques (see experimental section and figures S1-S5 in the electronic supplementary information (ESI)).

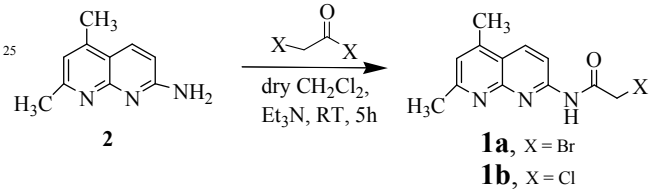

Scheme 1. General synthetic scheme for the synthesis of **1a** and **1b**.

The chemosensor **1a** (40 μM, CH_3CN) exhibited strong absorption bands at λ_{max} 328 and 239 nm. On addition of tetrabutylammonium fluoride (160 μM) to a solution of receptor **1a** (40 μM) in CH_3CN, exhibited a large red-shift in absorption spectrum (figure 1a) and consequently, an enhancement (fluorescence 'turn-on') in emission spectrum (figure 1b).

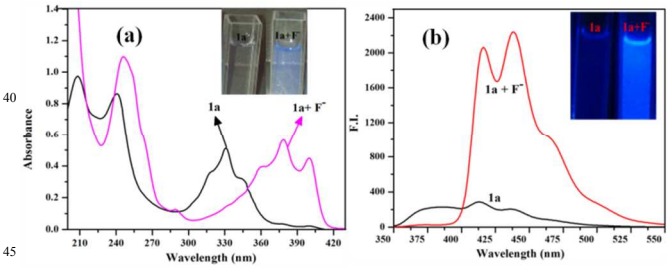

Figure 1. (a) UV spectral changes of **1a** (4×10^{-5} M) with 4 eq. F^- ions in CH_3CN; (b) Fluorescence spectra of **1a** (40 μM) in response to the presence of F^- ions (4 equiv.) in CH_3CN.

However, the addition of acetate ions showed smaller changes than that observed for F^- ions. The other anions, e.g., $H_2PO_4^-$,Cl^-, Br^-, I^-, HSO_4^-, PF_6^-, ClO_4^-, BF_4^- and NO_3^- caused no significant changes in the fluorescence and UV-Vis spectral features of **1a** (figures 2 and S6 in ESI).

On gradual addition of TBAF to a solution of **1a** (40 μM, CH_3CN), the absorbance at 328 nm underwent consequential decrease in its intensity with concomitant increase at 376 and 397 nm with an isobestic point at 334 nm (figure 3a). This red shift indicates the significant stabilization of the intramolecular charge transfer achieved through interaction of **1a** with fluoride ions.[19] Receptor **1a** (40 μM, CH_3CN) on excitation at 328/240nm exhibited emission bands at 390, 417 and 438 nm. Interestingly, on addition of fluoride ions (0 - 1.6×10^{-4} M), the fluorescence intensity gets enhanced (figure 3b). The sensor can also be used for colorimetric naked eye detection of F^- ions (figure S7 in ESI). Dilute solutions show blue florescence even in daylight. Enhancement of the blue fluorescent of **1a** (40 μM) was observed upon addition of TBAF under naked eye and under irradiation of long UV light (insets of figure 1). We propose that the excellent preference of receptor **1a** towards F^- ions is possibly due to deprotonation of amide –NH proton by F^- ion which results in the

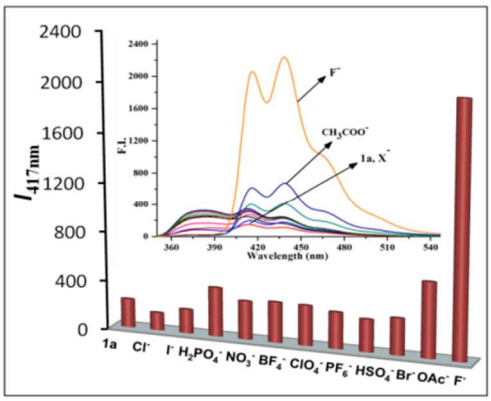

Figure 2. Fluorescence enhancement of receptor **1a** (40 μM) upon addition of different anions (4 equiv.) in CH_3CN. Inset: fluorescence spectra of **1a** upon addition of 4 equiv. of various anions.

formation of an anion of **1a,** i.e. $[\mathbf{1a}]^-$, which delineates the subtle difference in the affinity among other competing anionic analytes. Further, the anion of **1a** is stabilised by delocalization of π-electrons in the receptor moiety, which causes bathochromic shift in the absorption spectrum.[19] Similar changes both in absorption and emission spectra were obtained when a relatively strong base such as Bu_4NOH was employed (figures S8 and S9 in the ESI).

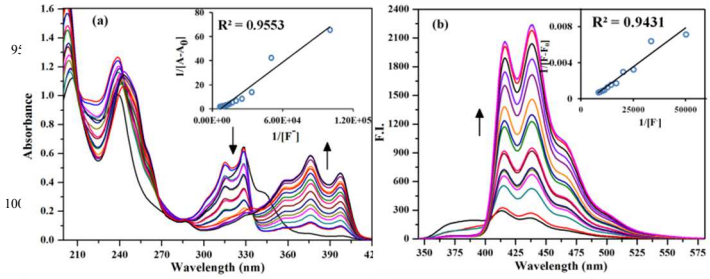

Figure 3. (a) Effect of incremental addition of $[F^-]$ on the UV-Vis spectrum of **1a** (40 μM); (b) Fluorescence spectral changes of **1a** by varying $[F^-]$ in CH_3CN. Insets: Benesi-Hildebrand plots for the respective titrations showing a 1:1 binding stoichiometry.

To confirm this assumption and evaluate the intermolecular interactions between the compound **1a** and fluoride ions, we carried out NMR studies in $CDCl_3$. It was found that on addition of tetrabutylammonium fluoride (TABF) to a solution of **1a** in $CDCl_3$ the amide proton completely disappeared indicating that the deprotonation of the -NH group is taking place in the presence of fluoride ions (figure S10 in ESI). To further support the effect of acidity of –NH proton on F^- ion binding, we have

synthesised receptor **1b** where control unit was -CH_2Cl. Interestingly, **1b** exhibited the similar spectral changes upon addition of F^- ions (figures S11-S14 in ESI). Also, fluoride ions didn't show any binding with starting material **2**, which contains only free -NH_2 group without any electron-withdrawing unit (figure S15 in ESI). Furthermore, ^{1}H-NMR spectrum showed amino proton resonance at δ 4.9 ppm in ligand **2**.[18] After attaching the halogen atom (-$COCH_2X$), the -NH proton shifts further downfield and resonates at ~δ 9.3ppm (**1a**), making it sufficiently acidic thereby interacting with carbonyl group through hydrogen bonding (supported by DFT), before the addition of anions. Thus, we can conclude that the presence of the more electronegative atoms in receptor **1a** and **1b** makes the amide protons relatively more acidic, F^- ion induced deprotonation of which results in both emission and absorption spectral changes.

Table 1. Deprotonation constants data[a] of Receptors **1a** and **1b** with F^- ions in CH_3CN.

Receptor	UV-Visible titration			Fluorescence titration		
	logK	K_a	n[b]	logK	K_a	n[b]
1a	3.84	6.93×10^3	1:1	3.76	5.97×10^3	1:1
1b	3.90	7.94×10^3	1:1	3.90	7.89×10^3	1:1

[a]Within the error ±0.01 for logβ_2 and ±2% for β_2; [b]n refers stoichiometry of receptor:anion host-guest complex.

Table 1 lists the deprotonation constatants data of receptors **1a** and **1b** in presence of F^- ions in CH_3CN at 298 K. On the basis of the UV-Vis titration profile (figures 3a and S12 in ESI) in the presence of externally added F^- ions, the deprotonation constants for **1a** and **1b** were found to be 6.93×10^3 M^{-1} and 7.94×10^3 M^{-1} with 1:1 stoichiometry. A systematic analysis (Benesi-Hildebrand plot) of the luminescent titration profiles (figures 3b and S14 in the ESI) support the formation of a 1:1 molecular assembly, while the deprotonation constant values of 5.97×10^3 M^{-1} (for **1a)** and 7.89×10^3 M^{-1} (for **1b)** were obtained. These values are in close proximity to the values obtained from the spectrophotometric titrations (table 1). The binding of 1:1 has also been confirmed by HRMS(ESI), where a peak corresponding to the 1:1 complex was observed (figures S16 and S17 in ESI).

To further understand the binding events of F^- ion with receptors, we have carried out computational studies.[17] There is hydrogen bonding interaction between amide NH and carbonyl CO both in gas phase as well as in CH_3CN exhibited by receptor **1a** and **1b** (figures 4 and S18 in ESI). The optimized structure for **1a•F$^-$** and **1b•F$^-$** clearly indicated that the addition of fluoride ion diminishes the hydrogen bonding interactions which can be attributed to the fact that fluoride ion being more basic interacts exceptionally well with the acidic amide hydrogen. Furthermore, the energy gap between the HOMO and LUMO of **1a•F$^-$** is smaller than that of sensing probe **1a**, which is in good agreement with the red shift in the absorption observed upon addition of fluoride ions to **1a**. However, as we move from gas phase to CH_3CN, the HOMOs become relatively more stabilized compared to their corresponding LUMOs (figures S19 and S20). To interpret further the absorption properties of **1a** and **1a•F$^-$** complexes, TD-DFT calculations were performed for these systems. As shown in table S1, the lowest energy transitions of **1a** arise from the HOMO → LUMO, HOMO-2 → LUMO+1 and HOMO-4 → LUMO+1 orbital transitions whereas the lowest energy transitions of **1a+F$^-$** originated from HOMO → LUMO,

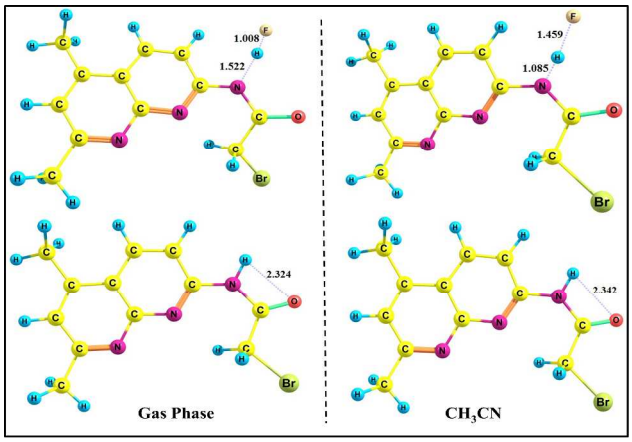

Figure 4. B3LYP/6-311+G(2df,2p) optimized geometries and important distances (Å) of **1a** and **1a•F$^-$** in gas phase and in CH_3CN.

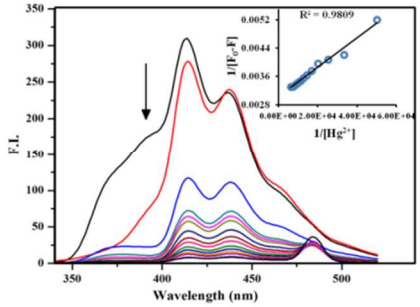

Figure 5. Fluorescence spectra of **1a** (40 μM) in the presence of varying [Hg^{2+}] in CH_3CN containing 0.8% of CH_3OH. Inset: Benesi–Hildebrand plot showing 1:1 binding stoichiometry.

HOMO and HOMO-3 → LUMO+2 orbital transitions as shown in figures S21 and S22, respectively in ESI. TD-DFT calculations provide a calculated absorption band that is consistent with the absorption band obtained experimentally (figure S23 in ESI).

Since the ligand has heteroaromatic binding sites, so the binding behaviour of receptor **1a** towards different cations cations (Na^+, Ag^+, Co^{2+}, Ni^{2+}, Cu^{2+}, Zn^{2+}, Cd^{2+}, Hg^{2+}, Pb^{2+} and Mn^{3+}) have been investigated by fluorescence spectroscopy. The gradual addition of Hg^{2+} ions (0-4 equiv.) resulted in quenching of fluorescence intensity as shown in figure 5. The other metal ions except Cu^{2+} didn't show any significant changes (figure 6a). The fluorescence spectral features of **1a** are identified by the presence of characteristic emission bands at 417 and 438 nm. After addition of Hg^{2+} ions, the intensity of these bands diminishes, indicating the interaction of Hg^{2+} ion with N1 and N8 atoms of naphthyridine moiety of the receptor **1a** (figure 6b). So, the observed fluorescence quenching (fluorescence 'turn-off') is possibly due to the combined effects of (i) energy- and/or electron-transfer processes, (ii) hindered π-delocalization by the binding of Hg^{2+} ion to 1,8-naphthyridine moiety, and (iii) heavy atom effect of Hg^{2+} ion.[20] The strong binding of Hg^{2+} ion towards **1a** was also reflected from binding constant data. The luminescent titration profile was fitting to a 1:1 binding model,

and the association constant (K_a) evaluated was found to be 7.28 × 10^4 M^{-1}. Further, this result was also confirmed by HRMS (ESI+), where a peak corresponding to 1:1 complex was observed (figure S24 in ESI).

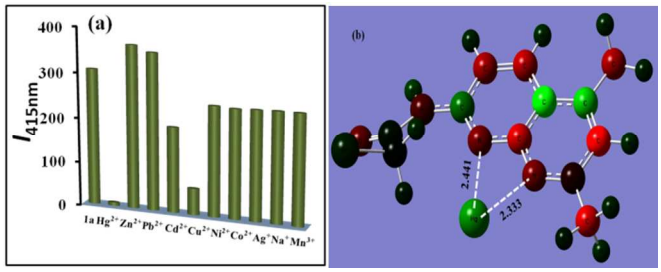

Figure 6. (a) Fluorescence response of receptor **1a** (40 µM) at 415 nm upon addition of different metal ions in CH_3CN containing 0.8% CH_3OH. (b) DFT Fully optimised structure of 1:1 **1a-Hg^{2+}** complex.

Fluorescence decay curves and Quantum yield:

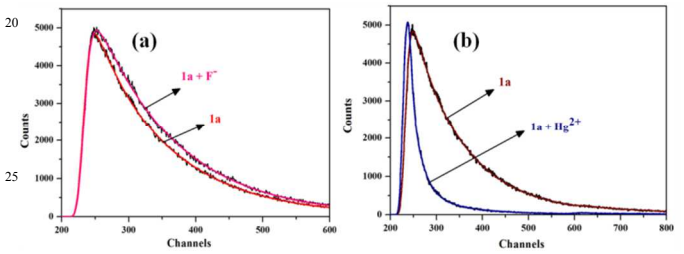

Figure 7. Fluorescence decay profile of **1a** in the absence and presence of (a) F^- (3 eq.) and (b) Hg^{2+} (4 equiv.) in CH_3CN medium.

1a•F$^-$ exhibited higher quantum yield (Φ_F = 0.89) than that of **1a** (Φ_F = 0.38). The fluorescence quantum yield (Φ_F) of receptor **1a** in the free and Hg^{2+}-bound state was found to be 0.38 and 0.032, respectively. These changes in the quantum yield were also correlated with the results of time resolved fluorescence studies. Time resolved fluorescence studies for **1a** in the absence and presence of F^- and Hg^{2+} ions has been done using a 280 nm LED as an excitation source in CH_3CN solution. The fluorescence lifetime increases from 6.02 ns (for **1a**) to 6.41 ns after addition of F^- ions. But in case of metal ion, lifetime decreases from 6.02 ns (for **1a**) to 1.74 ns (for **1a•Hg^{2+}**) as shown in figure 7, indicating the strong complexation of receptor **1a** with Hg^{2+} ion. These substantial changes in lifetimes and quantum yields of receptor **1a** in the presence of F^- and Hg^{2+} ions proved its credentials as a good sensor for these two ions.

Selectivity studies

Competitive binding studies were also performed to study the interference of the other anions and metal ions. Selectivity of probe is very crucial as the interference of other ions can affect its sensitivity. For the competitive binding studies equal concentration of Hg(II) and other metals were taken. In case of anions, anti-interference experiment has been carried out using double concentration of all interfering anions. Figures 8 and 9 showed that among the served metal ions no metal ion interferes with the Hg^{2+} and no anion interfere with selectivity of fluoride ion. Hence sensor **1a** acts as an excellent sensor even in presence of other metal ions and anions.

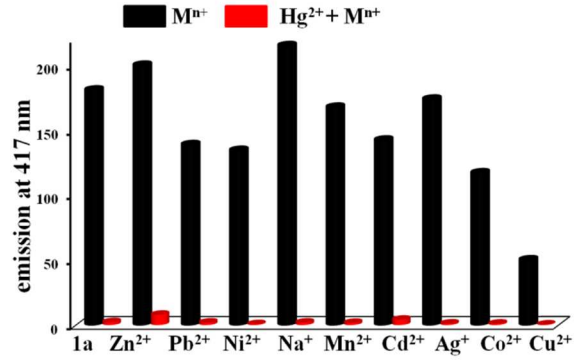

Figure 8. Selectivity of metal ions at wavelength 417 nm in a solution having **1a** + metal ions (black bar) and 1a + metal ions + Hg(II) (red bar) observed using fluorescence spectral studies

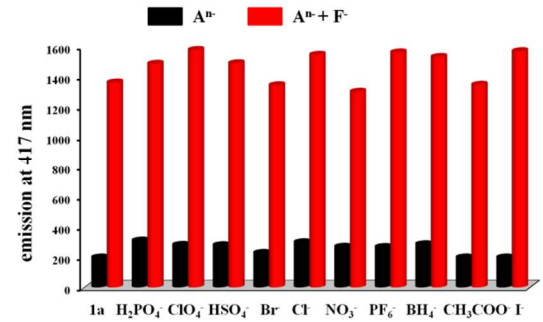

Figure 9. Selectivity of metal ions at wavelength 417 nm in a solution having **1a** + anions (black bar) and 1a + anions + F^- (red bar) observed using fluorescence spectral studies

Detection limit

The detection limit was determined from the absorption and fluorescence titration data based on a reported method. According to the result of titration experiment, the absorption and fluorescent data were normalized between the minimum and the maximum value. A linear curve was obtained from these data, and the point at which this line crossed the x-axis was considered as the detection limit.[21]

Table 2. The detection limits of fluoride and mercury ions exhibited by the receptors **1a** and **1b**.

Receptor	F^-		F^-		Hg^{2+}	
	UV-Vis titration		FL titration		FL Titration	
	µM	ppm	µM	ppm	µM	ppm
1a	22.9	0.43	28.8	0.55	11.9	2.4
1b	46.4	0.88	66.8	1.27	-	-

Table 2 lists the detection limits[21] of F^- and Hg^{2+} ions exhibited by the receptors **1a** and **1b**. They have shown excellent preference for fluoride ions with the detection limits of 2.29 × 10^{-5} M (0.43 ppm) and 4.64 × 10^{-5} M (0.88 ppm), respectively (figures S25 and S26 in ESI). **1a** was found to have high selectivity towards Hg^{2+} ions and a detection limit of 1.19 × 10^{-5} M (2.4 ppm), which is sufficiently low to allow the fluorimetric detection of nearly µm concentrations of Hg^{2+} ions (figure S27 in ESI).

Logic gate application

Based on the interaction of **1a** with F^- and Hg^{2+} ions with subsequent changes of its emission intensity at 438 nm, we have used our system for the construction of INHIBIT type combinatorial logic gate.[9,10] The output corresponds to the response of fluorescence emission at 438 nm. In order to elucidate the design of the logic gate, we assign logic 0 and logic 1 to the inputs and outputs. The four possible input combinations are (0, 0), (1, 0), (0, 1) and (1, 1) as shown in Table 3.

Table 3. Truth table for the INHIBIT logic gate.

Entry	Input 1 (F^-)	Input 2 (Hg^{2+})	Output (438 nm)
1	0	0	0
2	1	0	1
3	0	1	0
4	1	1	0

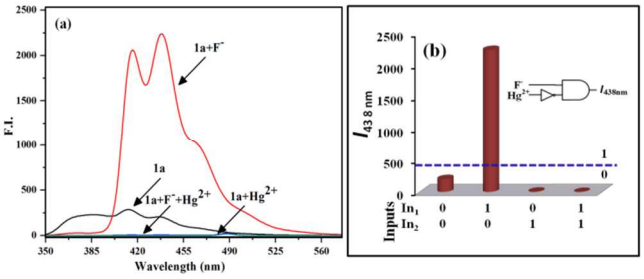

Figure 10. (a) Emission spectra of **1a** under different input conditions; (b) Output (fluorescence intensity at 438 nm) response to the absence and presence of F^- and Hg^{2+} ions.

It has been observed that in the presence or absence of both the input signals (F^-, Hg^{2+} = 1 or F^-, Hg^{2+} = 0) no output signals were obtained, whereas in the presence of the fluoride ion as only input signal (F^- = 1, Hg^{2+} = 0) enhanced fluorescence, as output signal was observed but reverse of that (F^- = 0, Hg^{2+} = 1) resulted in no output signal (figure 10). Thus, the logic circuit incorporating the truth table constitutes the two input INHIBIT logic gate that demonstrate a noncumulative behaviour that is, presence of Hg^{2+} (inverter) disable the whole system.

Summary of binding events

Sensor **1a** detects F^- ions *via* deprotonation mechanism leads to fluorescence enhancement, while the complex formation with Hg(II) leads to quenching of fluorescence.

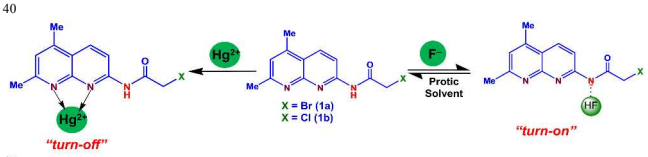

Scheme 2. Schematic representation of Hg^{2+} ion binding with **1a** and **1b** and F^- ion induced deprotonation of these receptors and their reversibility in presence of protic solvents.

The spectral changes observed in the presence of fluoride ions are not by the nucleophillic displacement of bromine of the bromoacetamido moiety. This is supported by carrying out the experiment in the presence of protic solvent. After addition of 4 eq. of F^- ions, the absorbance of **1a** at 328 nm underwent consequential decrease in its intensity with concomitant increase at 376 and 397 nm giving blue fluorescence, but when excess of fluoride ions are added, the peaks at 376 and 397 nm diminishes with the appearance of 307 nm and 425 nm bands and colour of the solution changes to yellow supporting the formation of complete anionic form of **1a** as shown in figure S28 and scheme S1 in ESI. When protic solvent methanol was added into this, the spectrum restored to original one. The same behaviour was observed with OH^- ions but sensor **1a** remains insensitive to Et_3N as shown in figure S29. So this observation completely removes the possibility of nucleophilic displacement of bromine of the bromoacetamido moiety by F^- ions.

Conclusions

In conclusion, we are reporting an elegant and modest synthetic route for 1,8-naphthyridine-based receptors which demonstrate the selective optical recognition of F^- and Hg^{2+} ions in two contrasting modes (fluorescence 'turn-on' and turn-off') with very low detection limits (0.5 - 2 ppm range). We explored the simple strategy that by appending halogen containing control unit (-$NHCOCH_2X$) on the fluorophore (1,8-naphthyridine) makes NH sufficiently acidic to sense small bronsted bases like F^- ions. The experimental results are in good accordance with computational studies (DFT and TD-DFT calculations). The chemical inputs (F^- and Hg^{2+} ions) generate an output which satisfy the condition of two-input INHIBIT logic operator. These results reported herein will pave a way to develop small molecule-based sensors for F^- and Hg^{2+} ions.

Experimental Section

General Information

All reagents were purchased from Alfa Aesar, HiMedia and were used without further purification. Acetonitrile (HPLC grade) was used to perform spectral studies. UV-Visible spectra were recorded on Agilent Cary 100 spectrophotometer, using a pair of quartz cells of 10 mm path length. The Fluorescence spectra were recorded on Hitachi F-4600 spectrofluorometer using a quartz cell of 10 mm path length. Excitation and emission slits are 5 nm/5 nm respectively. ^1H NMR spectra were recorded on Bruker AVANCE 500 MHz spectrometer in $CDCl_3$. Data are reported as follows: chemical shifts in ppm (δ), multiplicity (s = singlet, d = doublet, br = broad singlet m = multiplet), coupling constants *J* (Hz), integration, and interpretation. The elemental analyses were performed on Elementar vario EL III instrument. FT-IR spectra were recorded as KBr pellets using Perkin Elmer instrument. HRMS-ESI mass spectra were recorded on Bruker Daltanics micro-TOF mass spectrometer using CH_3CN as solvent. Fluorescence lifetime measurements were recorded on a Horiba Jobin Yvon 'FluoroCube Fluorescence Lifetime System' using a 280 nm LED as an excitation source in CH_3CN solution. Electrochemical measurements were carried out using CH instrument (CH 620E). The relative fluorescence quantum yields (ϕ) were estimated using equation 1 by using the integrated

emission intensity of 9,10-diphenyl anthracene (ϕ_{fr} = 0.90 in cyclohexane) as a reference.

$$\phi_{fs} = \phi_{fr} (I_{sample}/I_{std})(A_{std}/A_{sample})(\eta^2_{sample} / \eta^2_{std}) \quad \text{Eq. 1}$$

Where, ϕ_{fr} is the absolute quantum yield for the 9,10-diphenyl anthracene used as reference; I_{sample} and I_{std} are the integrated emission intensities; A_{sample} and A_{std} are the absorbance at the excitation wavelength, and η_{sample} and η_{std} are the refractive indices.

UV-Vis and fluorescence titrations

UV-Vis and fluorescence titrations were performed using freshly prepared 40 μM solution of ligands (**1a**, **1b** and **2**) in CH_3CN. To this, aliquots of freshly prepared solution (2×10^{-3} M) of tetrabutylammonium salts, TBAX where X = F^-, Cl^-, Br^-, I^-, ClO_4^-, PF_6^-, HSO_4^-, NO_3^-, BF_4^-, CH_3COO^-, $H_2PO_4^-$ were added in CH_3CN. For metal ion binding, we have prepared 2×10^{-3} M solution of various metal acetates [$M(CH_3COO)_x \bullet yH_2O$ where M = Co^{2+}, Cu^{2+}, Hg^{2+}, Zn^{2+}, Ni^{2+}, Cd^{2+}, Ag^+, Na^+ and Mn^{3+}; x = 1, 2 and 3; y = 1 and 2] in CH_3CN:MeOH mixture (24.8:0.2, v/v). The deprotonation and association constants as well as stoichoimetry were calculated using Benesi-Hildebrand plots.[22]

DFT Calculations

All calculations were carried out using density functional theory (DFT)[17] with Becke's three-parameter hybrid exchange functional and the Lee–Yang–Parr correlation functional abbreviated as B3LYP[23,24] level of theory. Analytical frenquency calculational were carried out on geometry optimized structure to ensure the minina on potential energy surface. The double-ζ basis set of Hav and Wadt (LanL2DZ) with a small core (1s2s2p3s3p3d4s4p4d) effective core potential (ECP)[25] was used for Hg. The ligand atoms H, N, C, O, Cl and Br were described using Pople's basis valence triple ζ with double polarization on all the atoms and diffusion on heavy atom i.e. using 6-311+G(2df,2p) basis set. All optimization calculations were performed with the Gaussian 09 (G09)[26] suite of programs. Solvent effects were accounted for by using CH_3CN (ε = 35.68) with a polarisable continuum model (PCM).[27] The absorption wavelengths and oscillator strengths were calculated using time-dependent density-functional theory (TD-DFT).[28]

Synthesis of receptors 1a and 1b

0.2 g (1.15 mmol) of 2-amino-5,7-dimethyl-1,8-naphthyridine (**2**)[29] was dissolved in dry CH_2Cl_2 and cooled to 0 ºC. To this, dry triethylamine (0.241 mL, 1.5 eq.) was added under argon atmosphere. Then haloacetyl halide (1.2 eq.) was added drop wise over a period of one hour and the resulting mixture was stirred at room temperature for 4 hrs. The precipitate formed was filtered, washed with CH2Cl2 and dried under vacuum. The yields were found to be 50% (0.170 g, 0.58 mmol) and 31% (0.09 g, 0.36 mmol) for **1a** and **1b**, respectively.

For **1a**: UV-Vis data ($\lambda/\varepsilon \times 10^{-3}$ L mol^{-1} cm^{-1}): 328 (16.32), 239 (31.41); Fl data (nm): 390, 417 and 438. ^{1}H NMR (500 MHz, $CDCl_3$, ppm): δ 2.68 (s, 3H; CH_3), 2.74 (s, 3H; CH_3), 4.08 (s, 2H; CH_2), 7.17 (s, 1H; Naph-H); 8.37 (d, J = 9Hz, 1H; Naph-H), 8.43 (d, J = 9Hz, 1H; Naph-H), 9.34 (br, 1H; NH); HRMS (ESI+): $C_{12}H_{13}BrN_3O$ $[M+H]^+$ Calcd.: 294.0242, Found: 294.0109; IR (KBr) ν_{max}: 619.2 cm^{-1}, 1415.4 cm^{-1}, 1558.9 cm^{-1}, 1617.9 cm^{-1}, 1639.0 cm^{-1}, 3416.2 cm^{-1}. Anal. Calcd for $C_{12}H_{12}BrN_3O$: C, 49.00; H, 4.11; N, 14.29. Found: C, 49.24; H, 4.38; N, 14.33.

For **1b**: UV-Vis data ($\lambda/\varepsilon\times10^{-3}$ Lmol^{-1}cm^{-1}): 328(10.50), 239(19.64); Fl data(nm): 375. ^{1}H NMR (500 MHz, $CDCl_3$, ppm): δ 2.79(s, 3H; CH_3), 2.97(s, 3H; CH_3), 4.30 (s, 2H; CH_2), 7.29 (s, 1H; Naph-H); 8.43 (d, J = 9Hz, 1H; Naph-H), 8.62 (d, J = 9Hz, 1H; Naph-H), 10.42 (br, 1H; NH); HRMS (ESI+): $C_{12}H_{13}ClN_3O$ $[M+H]^+$ Calcd: 250.074, Found: 250.072; $[M+Na]^+$ Calcd: 272.056, Found: 272.054. IR (KBr) ν_{max}: 643.5 cm^{-1}, 1412.1 cm^{-1}, 1558.3 cm^{-1}, 1641.2 cm^{-1}, 3450.2 cm^{-1}. Anal. Calcd for $C_{12}H_{12}ClN_3O$: C, 57.72; H, 4.84; N, 16.83. Found: C, 57.85; H, 4.95; N, 16.72.

We are grateful for the financial support provided by Council of Scientific and Industrial Research (01(2694)/12/EMR-II), Science and Engineering Research Board (SB/FT/CS-015/2012) and Board of Research in Nuclear Sciences (2012/37C/61BRNS/253). MKC thanks UGC, India for the SRF fellowship.

Notes and references

Department of Chemistry, Indian Institute of Technology Roorkee, Roorkee - 247667, India. Tel: +91-1332-28-4753; Fax: +91-1332-27-3560; E-mail: sankafcy@iitr.ac.in.

†Electronic Supplementary Information (ESI) available: UV-Vis., FL, NMR and mass spectra of **1a** and **1b**, UV-Vis and FL titrations, quantum yield and FL decay curves, LOD, DFT optimized geometries, pictorial views of FMOs, HOMO-LUMO diagrams and Cartesian coordinates for optimized geometries are available.

1 (a) P. A. Gale and C. Caltagirone, *Chem. Soc. Rev*., 2015 (DOI:10.1039/c4cs00179f). (b) F. Wang, L. Wang, X. Chen and J. Yoon, *Chem. Soc. Rev.,* 2014, **43,** 4312.

2 (a) D. S. Kim and J. L. Sessler, *Chem. Soc. Rev.*, 2014, DOI: 10.1039/c4cs00157e; (b) J. L. Sessler, P. A. Gale and W.-S. Cho, *Anion Receptor Chemistry*, RSC Publishing, Cambridge, UK, 2006; (c) P. D. Beer and P. A. Gale, *Angew. Chem., Int. Ed*., 2001, **40**, 486-516; (d) M. E. Moragues, R. Martinez-Manez and F. Sancenon, *Chem. Soc. Rev.,* 2011, **40,** 2593; (e) L. E. Santos-Figueroa, M. E. Moragues, E. Climent, A. Agostini, R. Martinez-Manez and F. Sancenon, *Chem. Soc. Rev.,* 2013, **42,** 3489; (f) R. Martinez-Manez and F. Sancenon, *Chem. Rev.,* 2003, **103,** 4419; (g) P.A. Gale, W. Dehaen and B.U.W. Maes, *Anion Recognition in Supramolecular Chemistry; Topics in Heterocyclic Chemistry*, *Vol. 24*, Springer-Verlag: Berlin, 2010. (h) M. Cametti and K. Rissanen, *Chem. Soc. Rev.,* 2013, **42,** 2016; (i) V. V. Roznyatovskiy, C.-H. Lee and J. L. Sessler, *Chem. Soc. Rev.*, 2013, **42**, 1921; (j) P. A. Gale and C.-H. Lee, *Top. Heterocycl. Chem.,* 2010, **24**, 39.

3 (a) H. N. Kim, W. X. Ren, J. S. Kim and J. Yoon, *Chem. Soc. Rev.,* 2012, 41, 3210; (b) Y. Jeong and *J. Yoon, Inorg. Chim. Acta.,* 2012, 381, 2; (c) N. Kaur and S. Kumar, *Tetrahedron.,* 2011, 67, 9233; (d) Z. Xu, J. Yoon and D. R. Spring, *Chem. Soc. Rev.,* 2010, 39, 1996; (e) S. Jing, C. Zheng, S. Pu, C. Fan and G. Liu, *Dyes Pigments,* 2014, 107, 38; (f) S. Pu, H. Ding, G. Liu, C. Zheng and H. Xu, *J. Phys. Chem. C,* 2014, 118, 7010; (g) S. Pu, D. Jiang, W. Liu, G. Liu and S. Cui, *J. Mater. Chem.,* 2012, 22, 3517; (h) S. Pu, Z. Tong, G. Liu and R. Wang, *J. Mater. Chem. C,* 2013, 1, 4726; (i) B. N. Ahamed , I. Ravikumar and P. Ghosh, *New J. Chem.,* 2009, 33, 1825; (j) Y. Lou, Y. Zhao, J. Chena and J.-J. Zhu, *J. Mater. Chem. C*, 2014, 2, 595; (k)

M. N. Alam, A. Chatterjee, S. Das, S. Batuta, D. Mandalb and N. A. Begum, RSC Adv., 2015, 5, 23419; (l) D. Karthiga and S. P. Anthony, RSC Advances, 2013, 3, 16765; (m) P. P. P. Kumar, C. H. Suresh and V. Haridas RSC Adv., 2015, 5, 7842; (n) A. Foroushani, Y. Zhang, D. Li, M. Mathesh, H. Wang, F. Yan, C. J. Barrow, J. Hee and W. Yang, Chem. Commun., 2015, 51, 2921.

4 (a) L. K. Kirk, Biochemistry of the Halogens and Inorganic Halides; Plenum Press: New York, 1991; (b) M. Kleerekoper, Endocrinol. Metab. Clin. North Am., 1998, 27, 441; (c) D. Briancon, Rev. Rhum. 1997, 64, 78; (d) Y. Michigami, Y. Kuroda, K. Ueda and Y. Yamamoto, Anal. Chim. Acta., 1993, 274, 299.

5 (a) Y. Zhou, J. F. Zhang and J. Yoon, *Chem. Rev.,* 2014, **114,** 5511; (b) C. Caltagirone and P. A. Gale, *Chem. Soc. Rev.,* 2009, **38,** 520; (c) D. A. Jose, D. K. Kumar, B. Ganguly and A. Das, *Org. Lett.,* 2004, **6,** 3445; (d) H. Zhao and F. P. Gabbai, *Nature Chem.,* 2010, **2,** 984; (e) S. P. Mahanta, B. S. Kumar, S. Baskaran, C. Sivasankar and P. K. Panda, *Org. Lett.,* 2012, **14,** 548; (f) S. Guha and S. Saha, *J. Am. Chem. Soc.,* 2010, **132,** 17674.

6 P.W. Davidson, G. J. Myers and B. Weiss, *Pediatrics*., 2004, **113,** 1023.

7 (a) J. Wang and X. Qian, *Chem. Commun.,* 2006, 109; (b) H. Zheng, Z-H. Qian, L. Xu, F-F. Yuan, L-D. Lan and J-G. Xu, *Org. Lett.,* 2006, 8, 859; (c) Y. Zhao and Z. Zhong, *J. Am.Chem. Soc.,* 2006, 128, 9988; (d) A. Dhir, V. Bhalla and M. Kumar, Org. Lett., 2008, 10, 4891; (e) M. Kumar, S. I. Reja and V. Bhalla, *Org. Lett.,* 2012, 14, 6084; (f) S. Saha, H. Agarwalla, H. Gupta, M. Baidya, E. Suresh, S. K. Ghosh and A. Das, *Dalton Trans.,* 2013, 42, 15097; (g) K. Bera, A. K. Das, M. Nag and S. Basak, *Anal. Chem.,* 2014, 86, 2740; (h) S. S. Ravi, L. R. Christena, N. SaiSubramanian and S. P. Anthony, *Analyst,* 2013, 138, 4370; (i) M. Caselli, *RSC Adv.,* 2015, 5, 1350 (j) P. Mahato, S. Saha, P. Das, H. Agarwalla and Amitava Das, *RSC Adv.*, 2014, 4, 36140; (k) Y. Si, X. Wang, Y. Li, K. Chen, J. Wang, J. Yu, H. Wang and B. Ding, *J. Mater. Chem. A,* 2014, 2, 645; (l) H. Lu, S. Qi, J. Mack, Z. Li, J. Lei, N. Kobayashi and Z. Shen, *J. Mater. Chem.,* 2011, 21, 10878.

8 A. P. de Silva, H. Q. N. Gunaratne, T. Gunnlaugsson, A. J. M. Huxley, C. P. McCoy, J. T. Rademacher and T. E. Rice, Chem. Rev., 1997, 97, 1515.

9 (a) J.-H. Lin and W.-L.Tseng, *Analyst.*, 2014, **139,** 1436-1441. (b) M. Zhang, H.-N. Le, X.-Q. Jiang and B.-C. Ye, *Chem. Commun.* , 2013, **49,** 2133; (c) B. Bag and P. K. Bharadwaj, *Chem. Commun.,* 2005, **24,** 513; (d) S. Chen, Z. Guo, S. Zhu, W.-e. Shi and W. Zhu, *ACS Appl. Mater. Interfaces.,* 2013, **5,** 5623; (e) M. Kluciar, R. Ferreira, B. de Castro and U. Pischel, *J. Org. Chem.,* 2008, **73,** 6079; (f) Y. Liu, M. Li, Q. Zhao, H. Wu, K. Huang and F. Li, *Inorg. Chem.* , 2011, **50,** 5969.

10 (a) A. P. de Silva and S. Uchiyama, *Nature Nanotech*., 2007, **2,** 399; (b) K. L. Kompa and R. D. Levine, *PNAS,* 2001, **98,** 410; (c) U. Pischel, *Angew. Chem. Int. Ed.,* 2007, **46,** 4026.

11 (a) C. Y. Hong, Y. K. Kim, J. H. Chang, S. H. Kim, H. Choi, D. H. Nam, Y. Z. Kim and J. H. Kwak, *J. Med. Chem.,* 1997, **40,** 3584; (b) K. Tomita, Y. Tsuzuki, K. Shibamori, M. Tashima, F. Kajikawa, Y. Sato, S. Kashimoto, K. Chiba and K. Hino, *J. Med. Chem.,* 2002, **45,** 5564; (c) P. L. Ferrarini, C. Mori, C. Manera, A. Martinelli, F. Mori, G. Saccomanni, P. L. Barili, L. Betti, G. Giannaccini, L. Trincavelli and A. Lucacchini, *J. Med. Chem.,* 2000, **43,** 2814; (d) Y. Tsuzuki, K. Tomita, K. Shibamori, Y. Sato, S. Kashimoto and K. Chiba, *J. Med. Chem.,* 2004, **47,** 2097.

12 (a) K. Nakatani, S. Sando, H. Kumasawa, J. Kikuchi and I. Saito, *J. Am. Chem. Soc.,* 2001, **123,** 12650; (b) K. Nakatani, S. Sando and I. Saito, *J. Am. Chem. Soc.,* 2000, **122,** 2172.

13 (a) J. M. Casas, B. E. Diosdado, J. Fornies, A. Martin, A. J. Rueda and A. G. Orpen, *Inorg. Chem.,* 2008, **47,** 8767; (b) U. Monkowius, Y. N. Svartsov, T. Fischer, M. Zabel and H. Yersin, *Inorg. Chem. Comm.,* 2007, **10,** 1473; (c) B. R. Yeo, A. J. Hallett , B. M. Kariuki and S. J.A. Pope, *Polyhedron,* 2010, **29,** 1088.

14 (a) K. Ghosh, T. Sen and R. Frohlich, *Tetrahedron Lett.,* 2007, **48,** 2935; (b) K. Ghosh, A. R. Sarkar and T. Sen, *Supramol. Chem.,* 2010, **22,** 81; (c) J. Kong , C. He, X. Zhang, Q. Meng and C. Duan, *Dyes Pigm.* , 2014, **101,** 254; (d) K. Ghosh, T. Sen, A. Patra, J. S. Mancini, J. M. Cook and C. A. Parish, *J. Phys. Chem. B*., 2011, **115,** 8597.

15 (a) Z. Li, W. Zhao, X. Li, Y. Zhu, C. Liu, L. Wang, M. Yu, L. Wei, M. Tang and H. Zhang, *Inorg. Chem.,* 2012, **51,** 12444; (b) M.-M.Yu, Z.-X. Li, L.-H. Wei, D.-H. Wei and M.-S.Tang, *Org. Lett.,* 2008, **10,** 5115; (c) X. Liu, M. Chen, Z. Liu, M. Yu, L. Wei and Z. Li, *Tetrahedron*., 2014, **70,** 658; (d) Y. Zhou, Y. Xiao and X. Qian, *Tetrahedron Lett.,* 2008, **49,** 3380; (e) P. Xie, Y. Xiao, D. Yao, Q. Jin and F. Guo, *J Fluoresc*., 2013, **23,** 265; (f) Z. Li, M. Yu, L. Zhang, M. Yu, J. Liu, L. Wei and H. Zhang, *Chem. Commun.,* 2010, **46,** 7169.

16 J.-H. Huang, W.-H. Wen, Y.-Y. Sun, P.-T. Chou, and J.-M. Fang, *J. Org. Chem.* 2005, **70,** 5827; (h) A. K. Mahapatra, G. Hazra, N. K. Das, P. Sahoo, S. Goswami and H.-K. Fun, *J. Photochem. Photobiol. A.,* 2011, **222,** 47.

17 R. G. Parr and W. Yang, *Density Functional Theory of Atoms and Molecules*; Oxford University Press: Oxford, U.K., 1989.

18 (a) L. Váradi, M. Gray, P. W. Groundwater, A. J. Hall, A. L. James, S. Orenga, J. D. Perry and R. J. Anderson, *Org. Biomol. Chem.,* 2012, **10,** 2578. (b) J. Bernstein, B. Stearns, E. Shaw and W. A. Lott, *J. Am. Chem. Soc.,* 1947, **69,** 1151.

19 S. K. Kim, J. H. Bok, R. A. Bartsch, J. Y. Lee and J. S. Kim, *Org. Lett.,* 2005, **7,** 4839.

20 H.-Y. Gong, Q.-Y. Zheng, X.-H. Zhang, D.-X. Wang and M.-X. Wang, *Org. Lett.,* 2006, **8,** 4895.

21 (a) M. Shortreed, R. Kopelman, M. Kuhn and B. Hoyland, *Anal. Chem*., 1996, **68,** 1414; (b) W. Lin, L. Yuan, Z. Cao, Y. Feng and L. Long, *Chem. Eur. J.,* 2009, **15,** 5096.

22 H. A. Benesi and J. H. Hildebrand, *J. Am. Chem. Soc.,* 1949, **71,** 2703.

23 C. Lee, W. Yang and R. G. Parr, *Phys. Rev. B,* 1998, **37,** 785.

24 A. D. Becke, *J. Chem. Phys*., 1993, **98,** 5648.

25 (a) P. J. Hay and W. R. Wadt, J. Chem. Phys., 1985, 82, 270 (b) W. R. Wadt and P. J. Hay, J. Chem. Phys., 1985, 82, 284 (c) P. J. Hay and W. R. Wadt, J. Chem. Phys., 1985, 82, 299.

26 Gaussian 09, Revision A.02; M. J. Frisch, G. W. Trucks, H. B. Schlegel, G. E. Scuseria, M. A. Robb, J. R. Cheeseman, G. Scalmani, V. Barone, B. Mennucci, G. A. Petersson, H. Nakatsuji, M. Caricato, X. Li, H. P. Hratchian, A. F. Izmaylov, J. Bloino, G. Zheng, J. L. Sonnenberg, M. Hada, M. Ehara, K. Toyota, R. Fukuda, J. Hasegawa, M. Ishida, T. Nakajima, Y. Honda, O. Kitao, H. Nakai, T. Vreven, J. A. Montgomery, Jr., J. E. Peralta, F. Ogliaro, M. Bearpark, J. J. Heyd, E. Brothers, K. N. Kudin, V. N. Staroverov, R. Kobayashi, J. Normand, K. Raghavachari, A. Rendell, J. C. Burant, S. S. Iyengar, J. Tomasi, M. Cossi, N. Rega, J. M. Millam, M. Klene, J. E. Knox, J. B. Cross, V. Bakken, C. Adamo, J. Jaramillo, R. Gomperts, R. E. Stratmann, O. Yazyev, A. J. Austin, R. Cammi, C. Pomelli, J. W. Ochterski, R. L. Martin, K. Morokuma, V. G. Zakrzewski, G. A. Voth, P. Salvador, J. J. Dannenberg, S. Dapprich, A. D. Daniels, O. Farkas, J. B. Foresman, J. V. Ortiz, J. Cioslowski, and D. J. Fox, Gaussian, Inc., Wallingford CT, 2009.

27 (a) J. Tomasi and M. Persico, *Chem. Rev.,* 1994, **94,** 2027; (b) V. Barone and M. Cossi, *J. Phys. Chem. A.,* 1998, **102,** 1995.

28 (a) D. Guillaumont and S. Nakamura, *Dyes Pigm.,* 2000, **46,** 85; (b) D. D. Censo, S. Fantacci, F. D. Angelis, C. Klein, N. Evans, K. Kalyanasundaram, H. J. Bolink, M. Gra1tzel and M. K. Nazeeruddin, *Inorg. Chem.* 2008, **47,** 980.

29. (a) T. R. Kelly, C. Zhao and G. J. Bridger, *J. Am. Chem. Soc.,* 1989, **111,** 3744; (b) T. R. Kelly, G. J. Bridger and C. Zhao, *J. Am. Chem. Soc.*, 1990, **112,** 8024.

Graphical Abstract

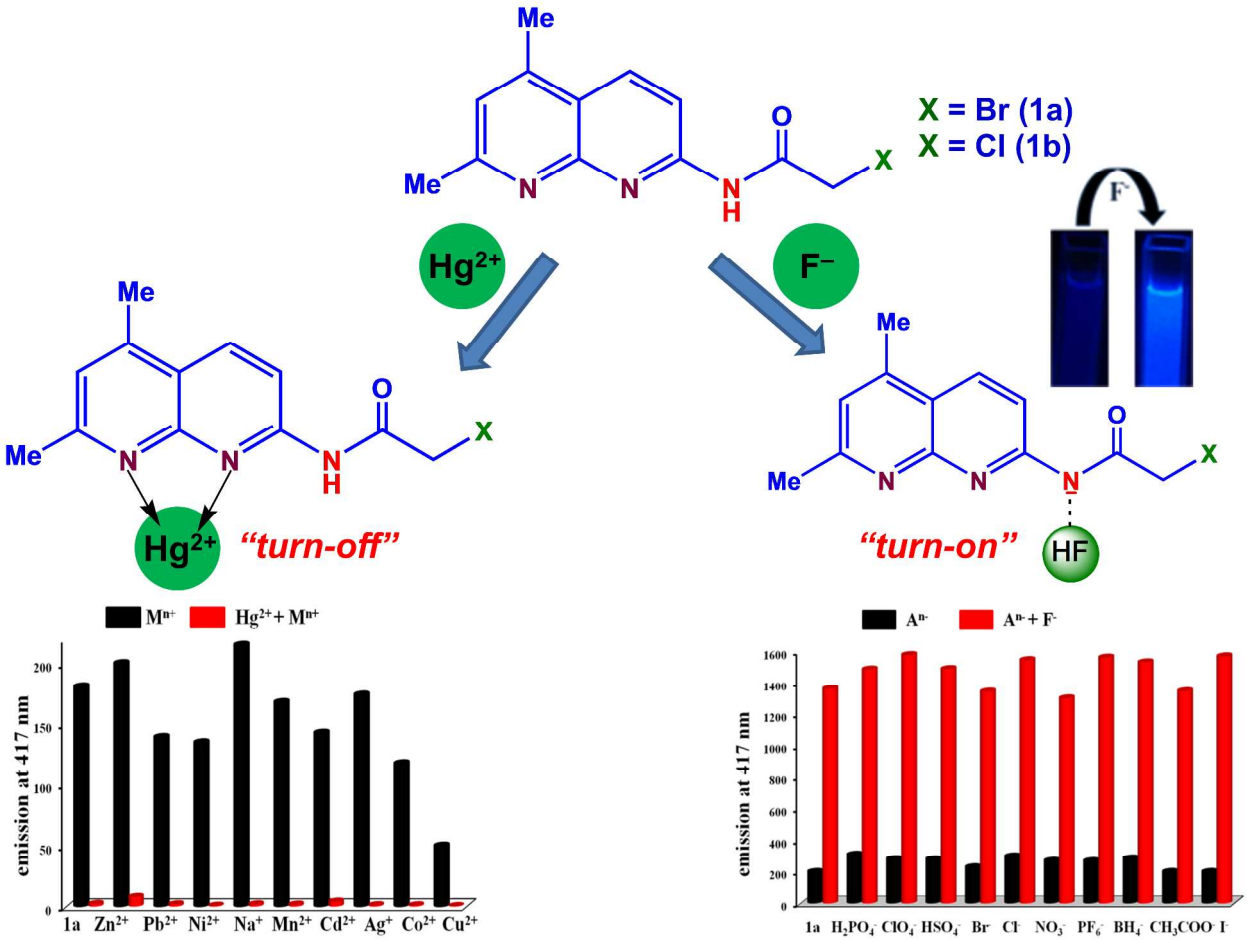

A highly selective naphthyridine-based fluorescent chemosensor has been designed and synthesized. The probe gave selective dual-channel response to detect F^- and Hg^{2+} ions with lower detection limits (0.5 - 2 ppm range). The chemical inputs of F^- and Hg^{2+} ions generate an output which satisfies the condition of two-input INHIBIT logic operator.

Electronic Supplementary Information for

1,8-Naphthyridinic fluorescent 'turn-on' and 'turn-off' chemosensors for detecting of F^- and Hg^{2+} mimicking INHIBIT molecular logic behaviour

Mandeep K. Chahal and Muniappan Sankar*

Department of Chemistry, Indian Institute of Technology Roorkee, Roorkee – 247667, India

E-mail: *sankafcy@iitr.ac.in*

Table of Contents

Table S1. Computed vertical excitation wavelength and their orbital contribution using B3LYP/6-311+G(2df, 2p) 14

Scheme S1. Schematic representation of binding events while adding 4 equivalents of F^- ions to **1a** and its regeneration upon addition of protic solvents such as methanol. 17

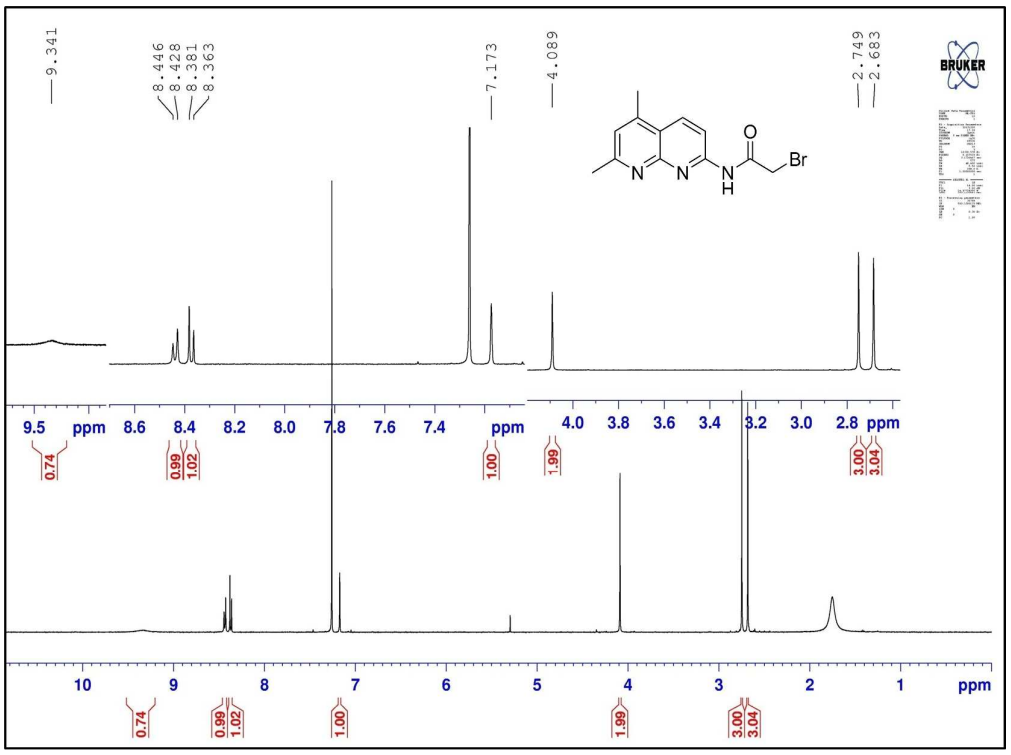

Figure S1. ^{1}H NMR spectrum of **1a** in $CDCl_3$.

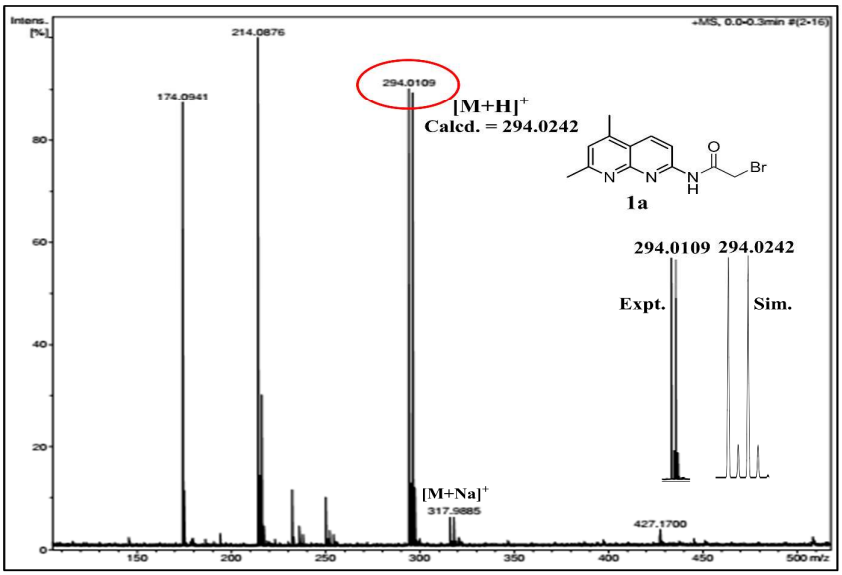

Figure S2. HRMS (ESI+) mass spectrum of **1a** in CH_3CN.

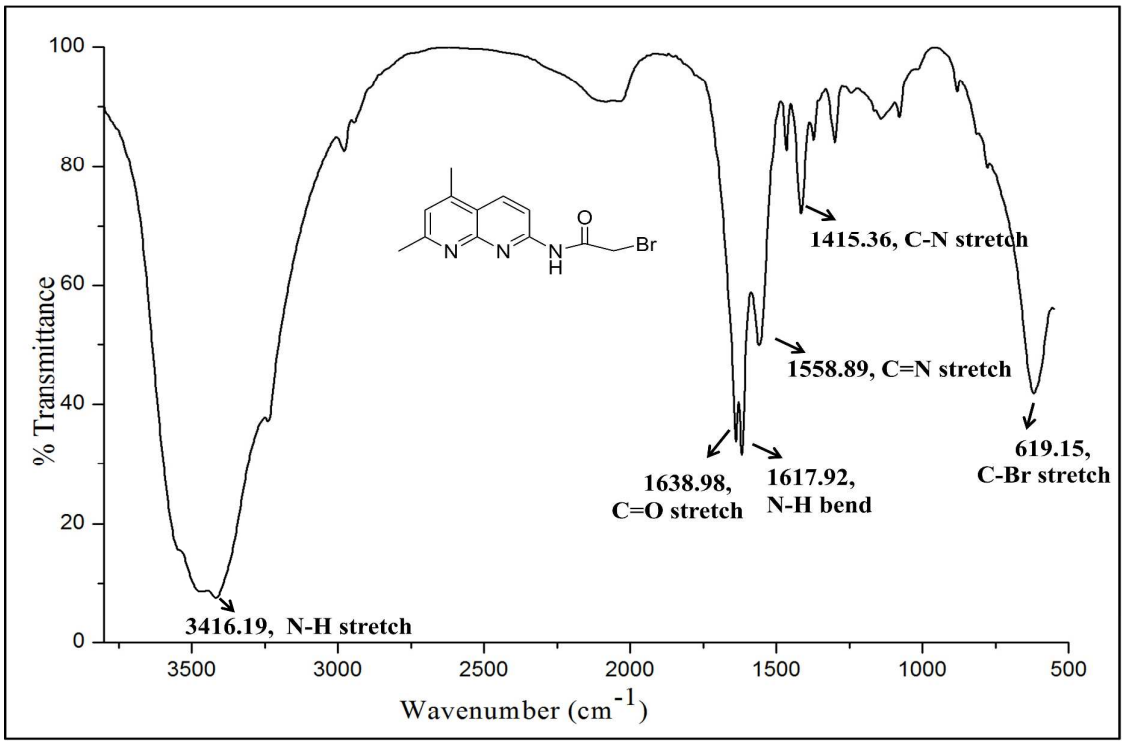

Figure S3. FT-IR spectrum of **1a** in KBr pellet.

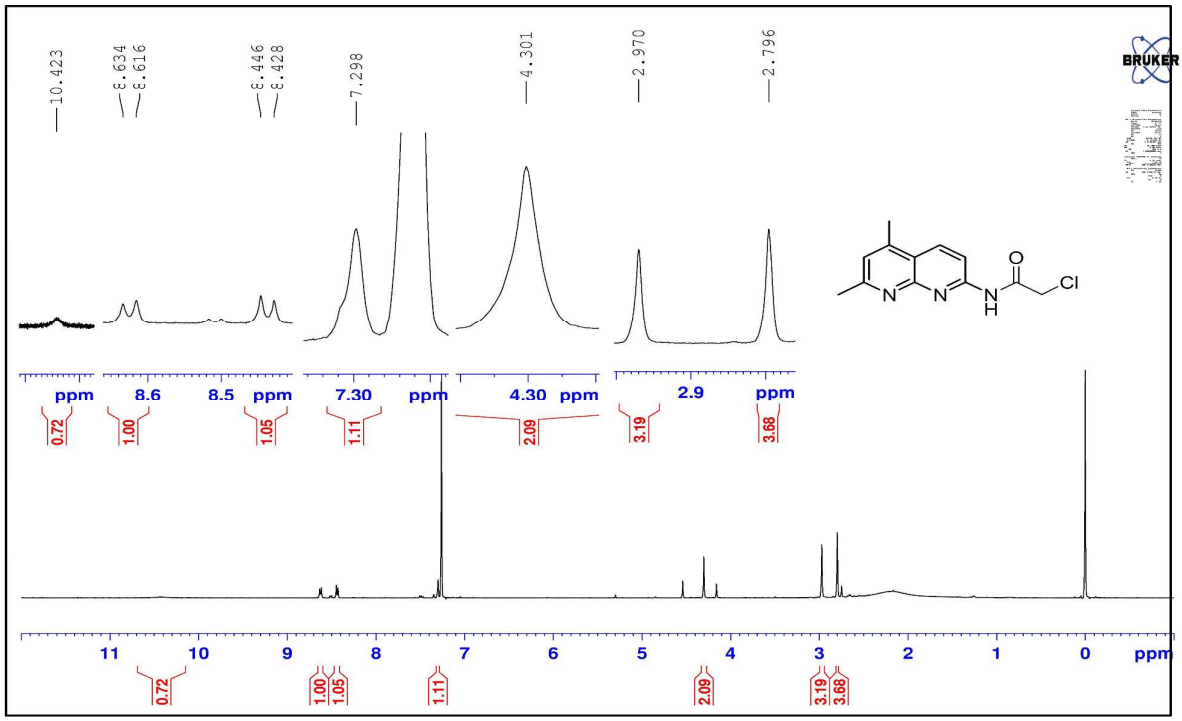

Figure S4. ^{1}H-NMR spectrum of **1b** in CDCl3.

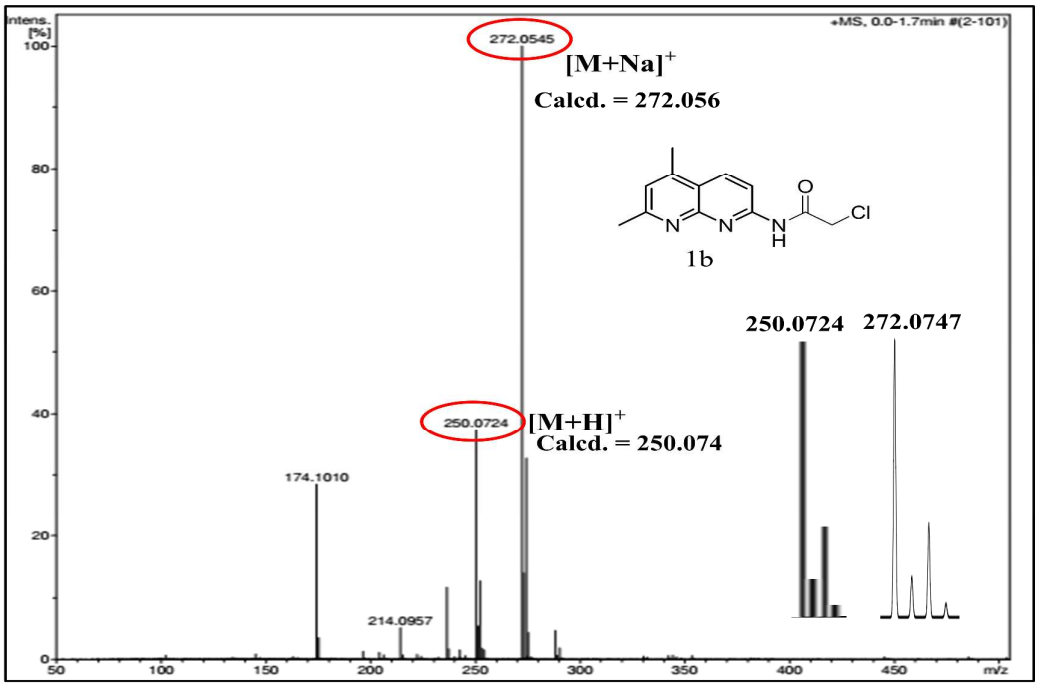

Figure S5. HRMS (ESI+) spectrum of **1b** in CH_3CN.

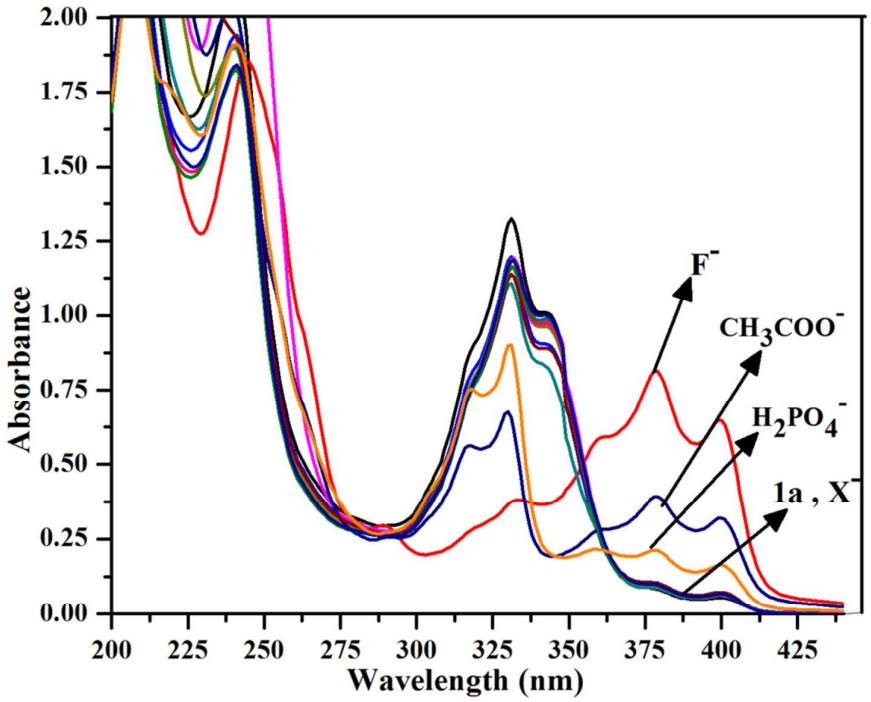

Figure S6. UV-Visible spectral changes of receptor **1a** (40 μM) upon addition of different anions (4 eq.) in CH_3CN at 298 K.

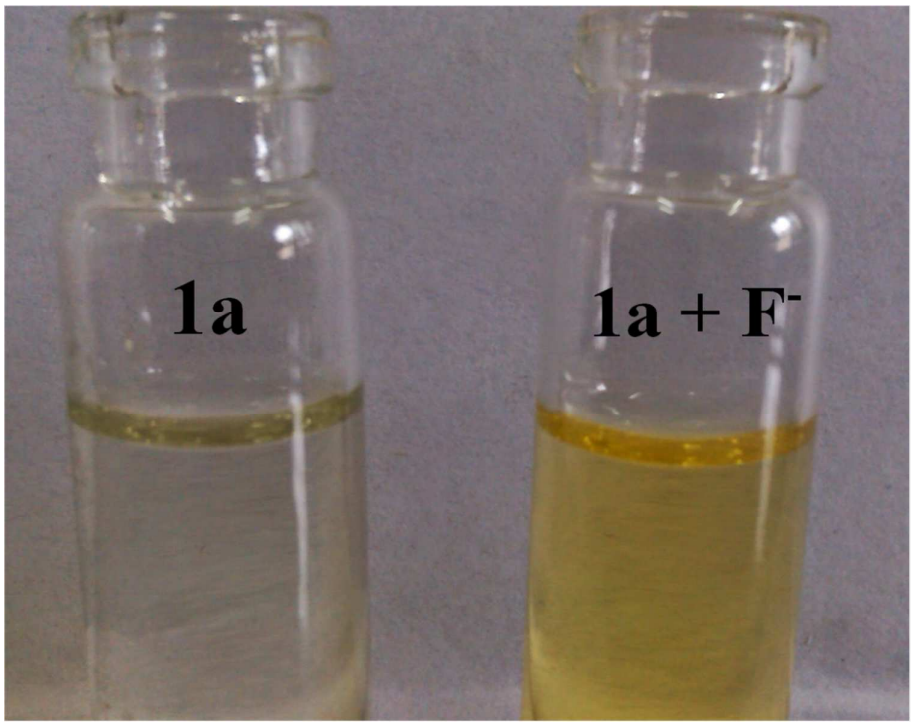

Figure S7. Colorimetric naked eye detection upon addition of fluoride ions in CH_3CN.

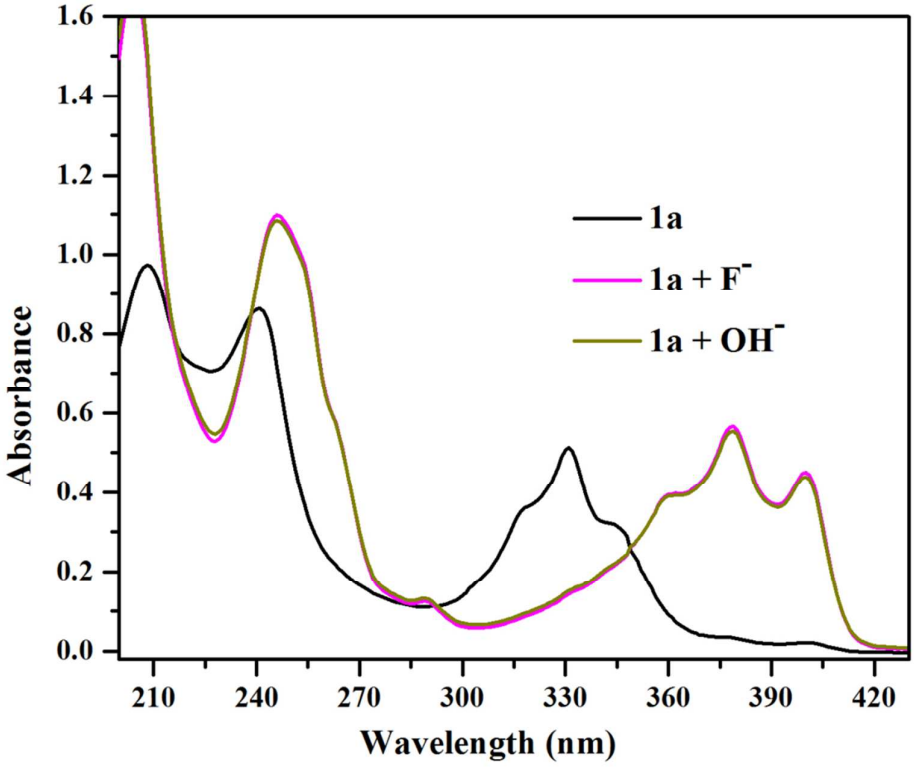

Figure S8. UV-Vis spectra of **1a** (40 μM), after the addition of F^- ion (120 μM) and strong base TBAOH (80 μM).

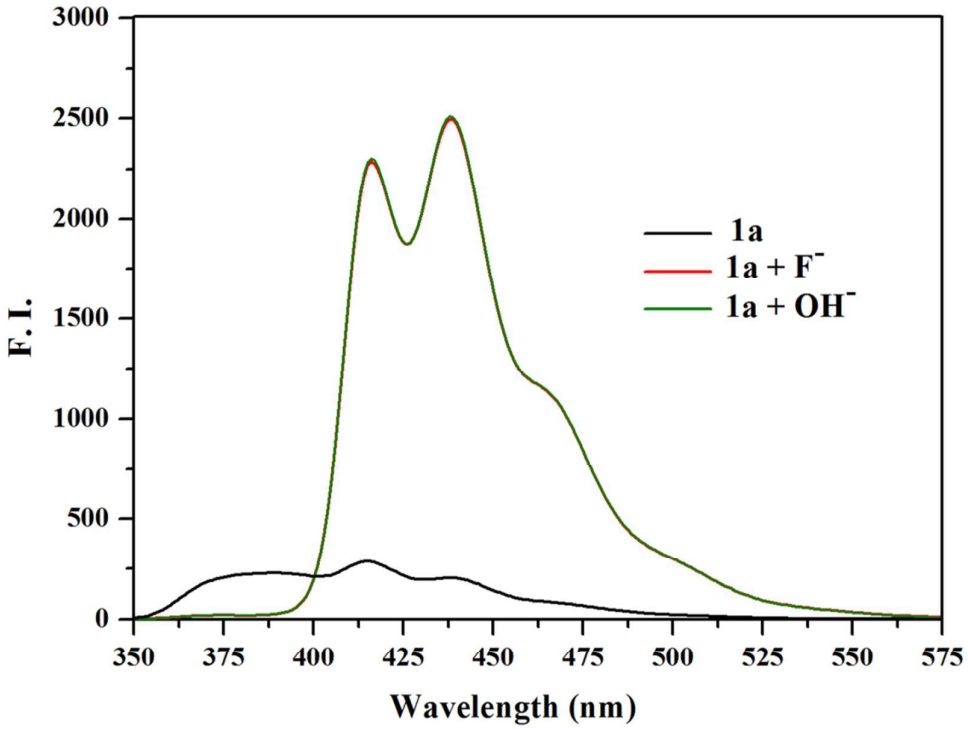

Figure S9. The fluorescence spectra of **1a** (40 μM), and after the addition of F^- (120 μM) and TBAOH (80 μM) supporting the deprotonation of amide NH-proton.

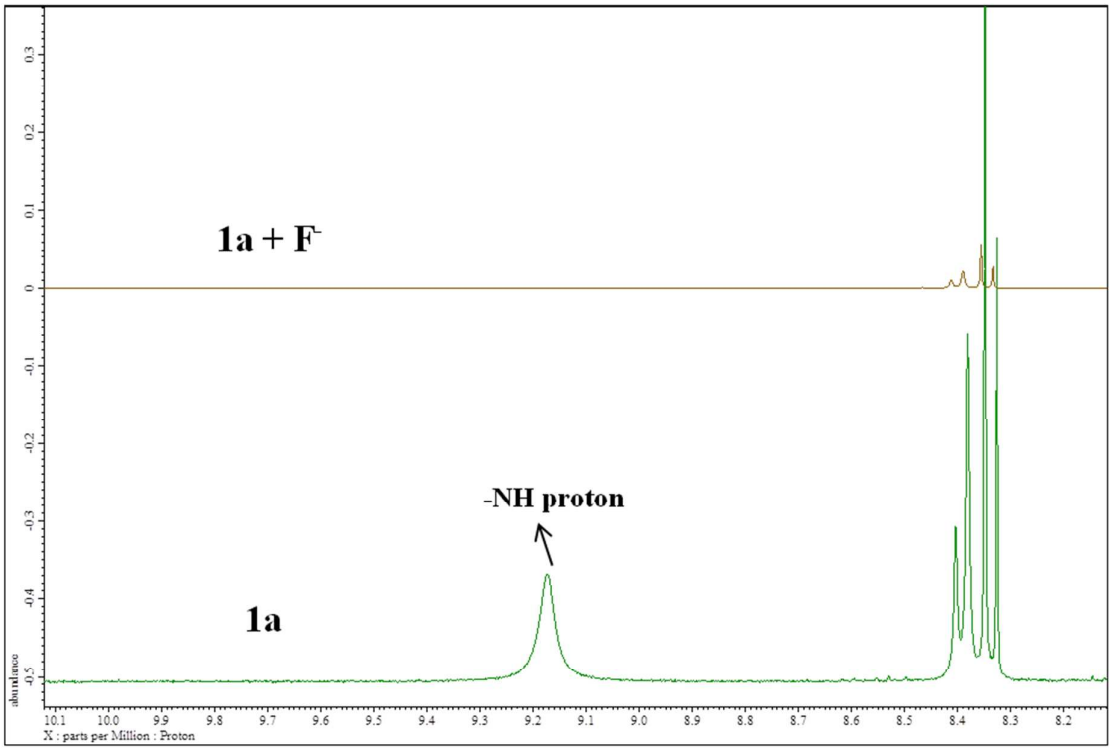

Figure S10. Overlay of NMR spectra of **1a** (0.01 M) in presence and absence of 4 equivalents of F^- ions in $CDCl_3$ at 298 K.

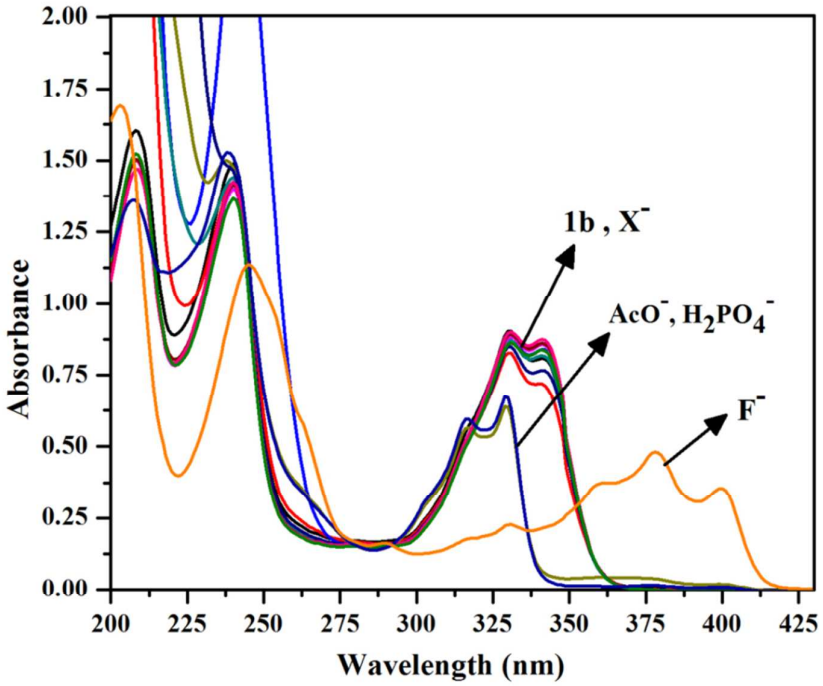

Figure S11. Absorption spectra of receptor **1b** (4 x 10^{-5} M) upon addition of 3 eq. of TBA salt of different anions in CH_3CN (X^- = Cl^-, Br^-, PF_6^-, ClO_4^-,I^- HSO_4^-, NO_3^- and BF_4^-).

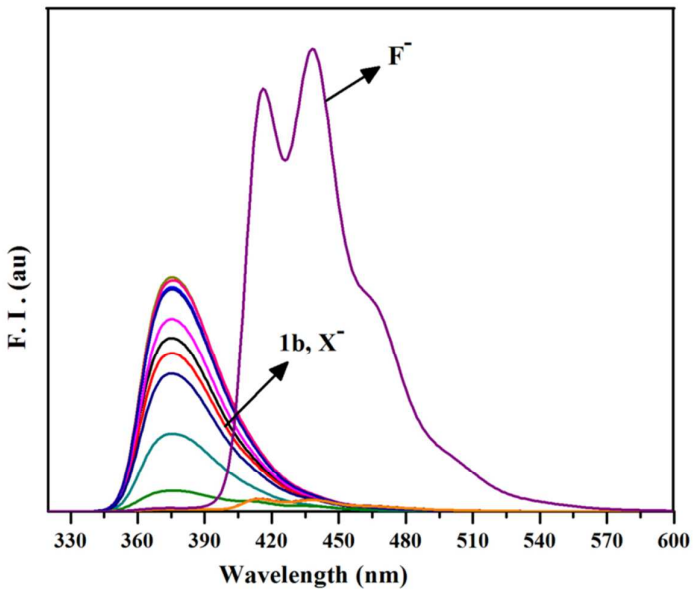

Figure S12. Fluorescence spectra of **1b** (4 × 10^{-5} M) in the absence and presence of 3 eq. of TBA salt of different anions in CH_3CN medium (X^- = CH_3COO^-, $H_2PO_4^-$,Cl^-, Br^-, I^-, HSO_4^-, PF_6^-, ClO_4^-, BF_4^- and NO_3^-).

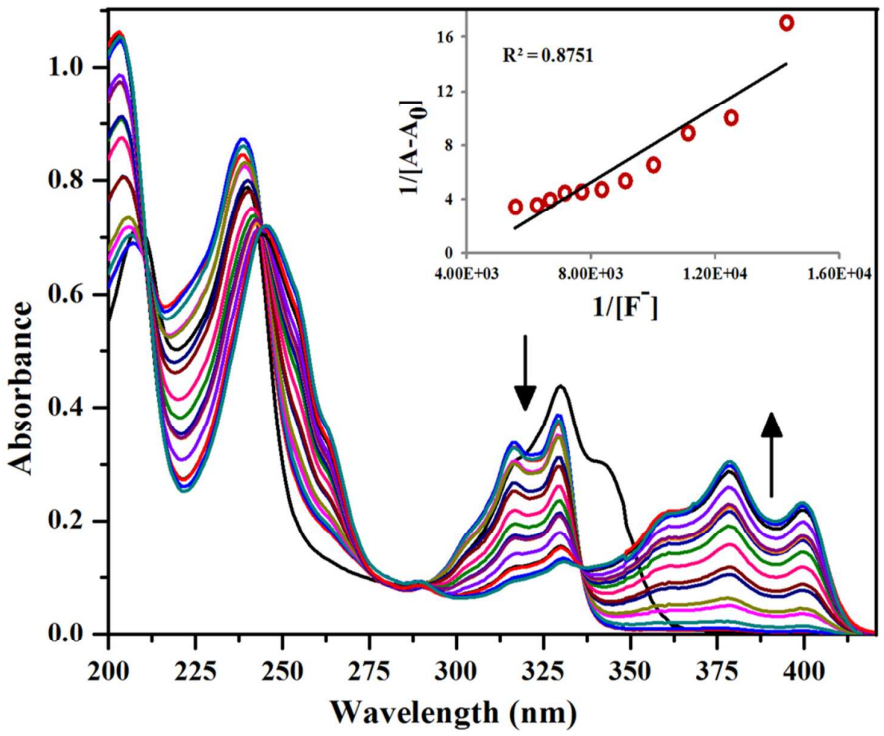

Figure S13. Absorption spectra of **1b** (4.0×10^{-5} M) in presence of varying concentration of F^- (0 to 1.60×10^{-4} M) in CH_3CN medium. Inset: Benesi-Hildebrand plot of **1b** with F^- ion when monitoring absorbance changes at 378 nm show the 1:1 stoichiometry.

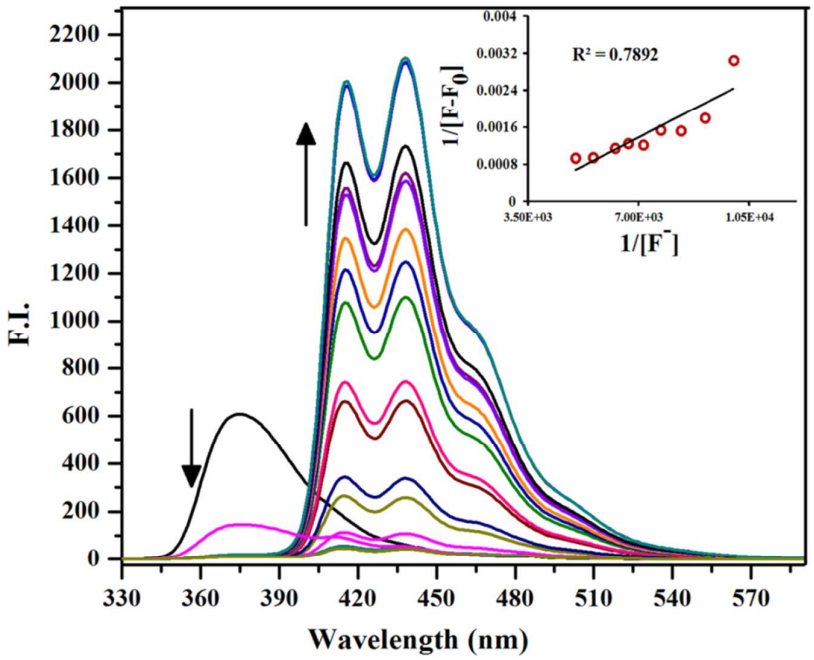

Figure S14. Emission spectral responses of **1b** (4.0×10^{-5} M) towards varying [F^-] (0 to 1.6×10^{-4} M) in CH_3CN. Inset: Good linear fit of Benesi-Hildebrand plot confirms the 1: 1 binding stoichiometry using λ_{ext} = 240 nm and λ_{mon} = 463 nm. Slit width 5 nm.

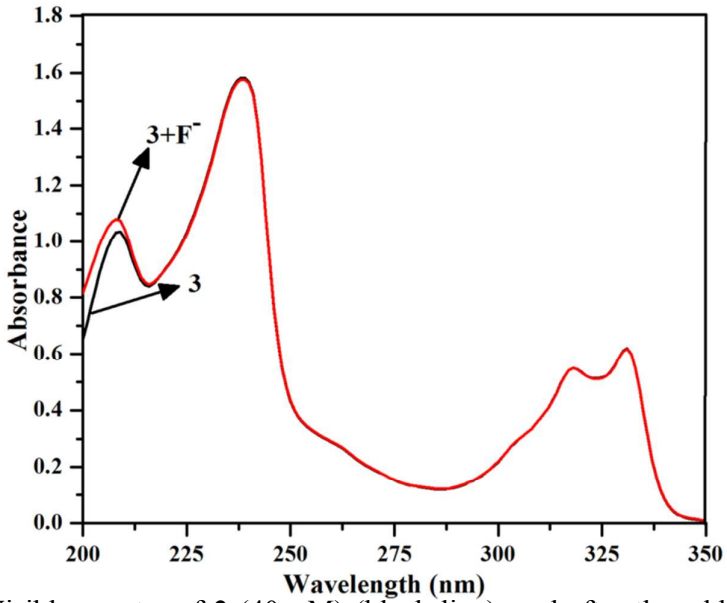

Figure S15. UV-Visible spectra of **2** (40 μM) (black line), and after the addition of F^- ion (120 μM) (red line) in CH_3CN.

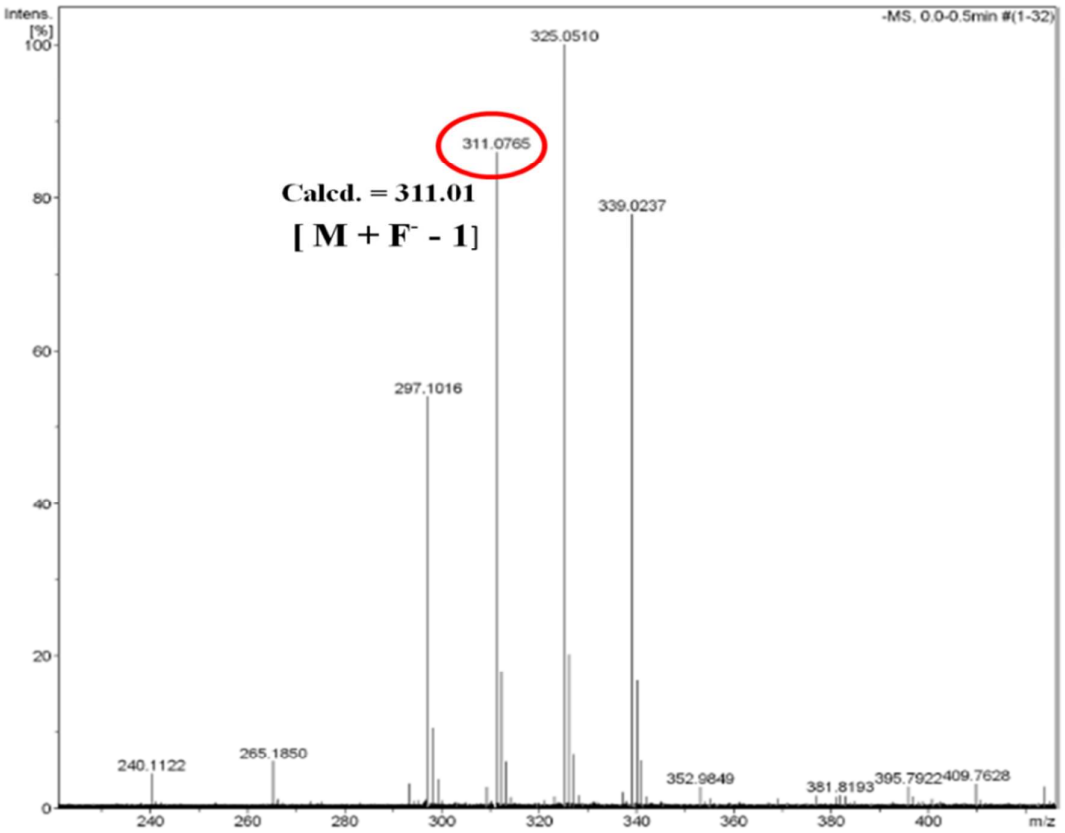

Figure S16. HRMS (ESI-) mass spectra of (1:1) complex of **1a** and fluoride ion.

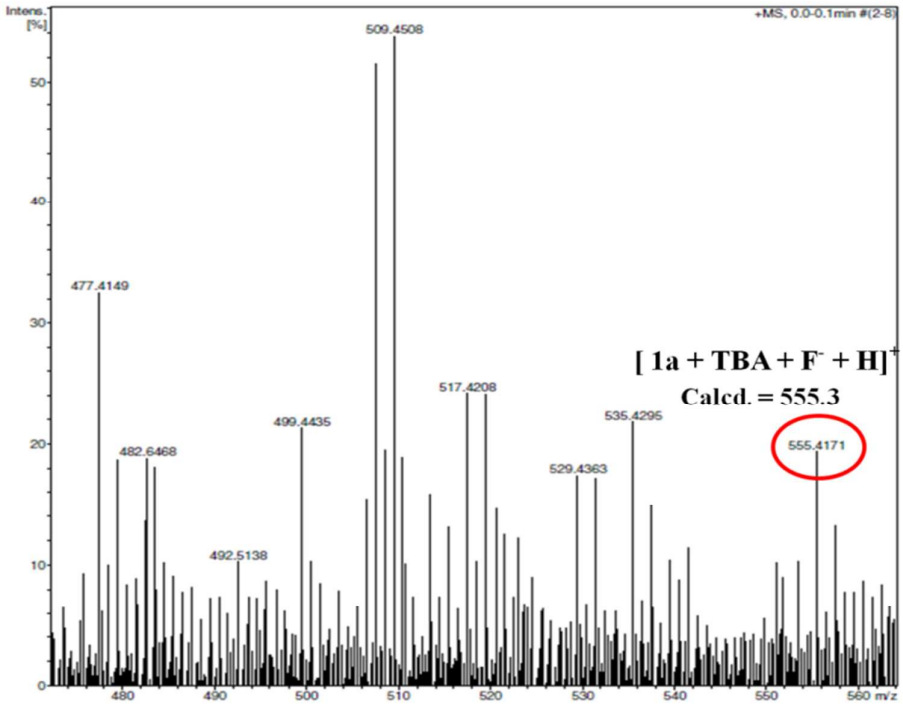

Figure S17. HRMS (ESI+) mass spectrum of (1:1) complex of **1a** and fluoride ion.

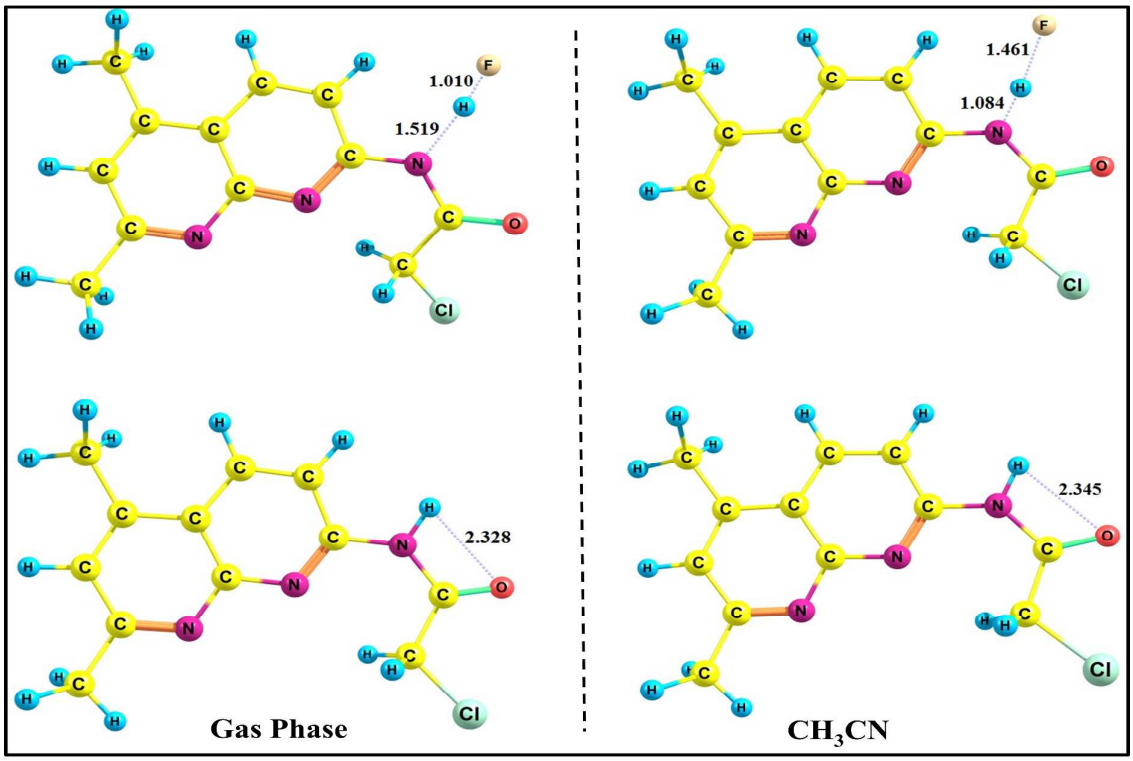

Figure S18. DFT-optimized structures of **1b** along with its fluoride complex in Gas phase and in CH_3CN calculated at B3LYP/6-311+G(2df,2p) level of theory.

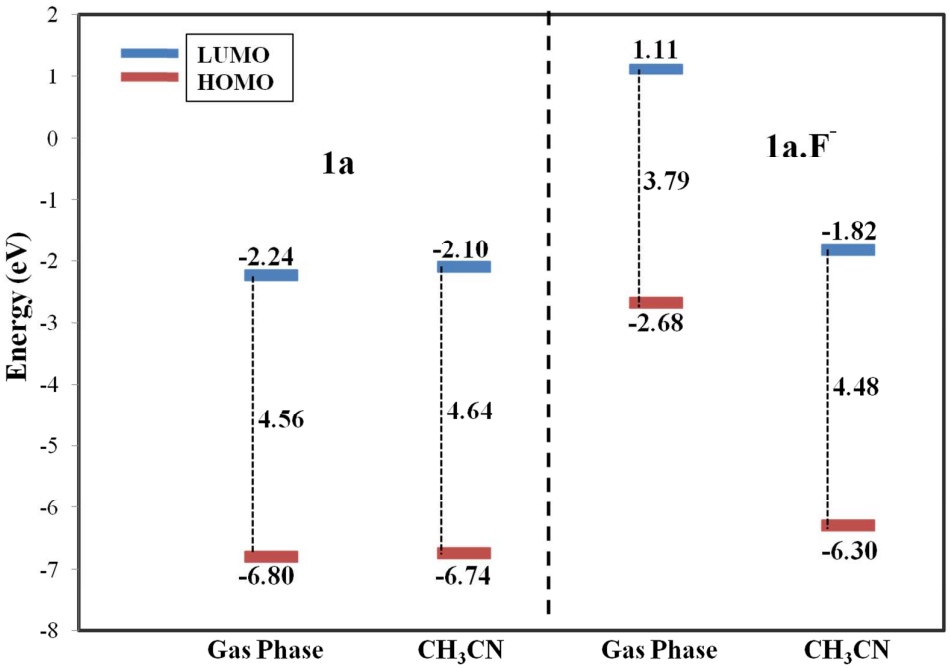

Figure S19. HOMO-LUMO energy gaps for **1a** and **1a+F**$^-$ complex in gas phase and CH_3CN.

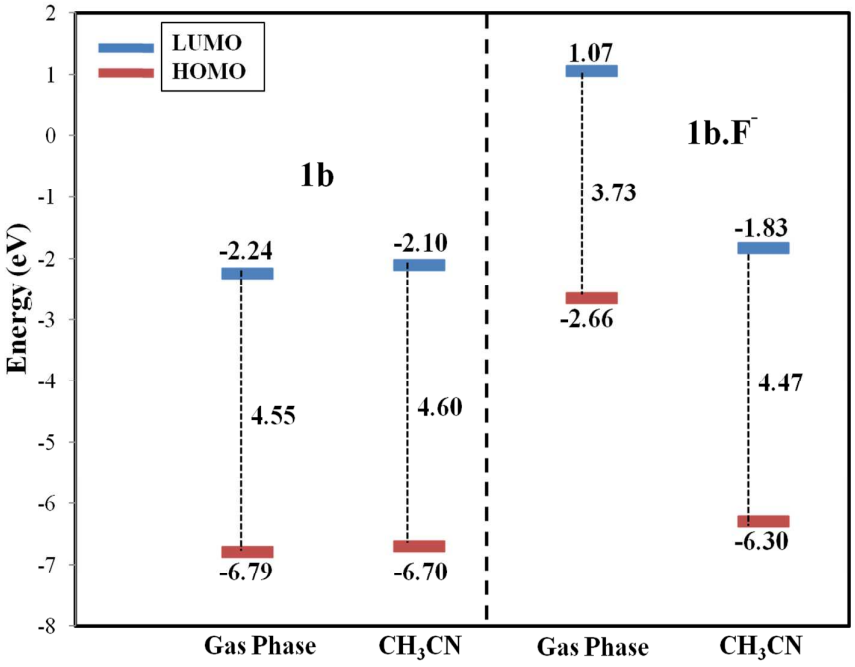

Figure S20. HOMO-LUMO energy gap for **1b** and **1b+F**$^-$ complex in gas phase and CH_3CN.

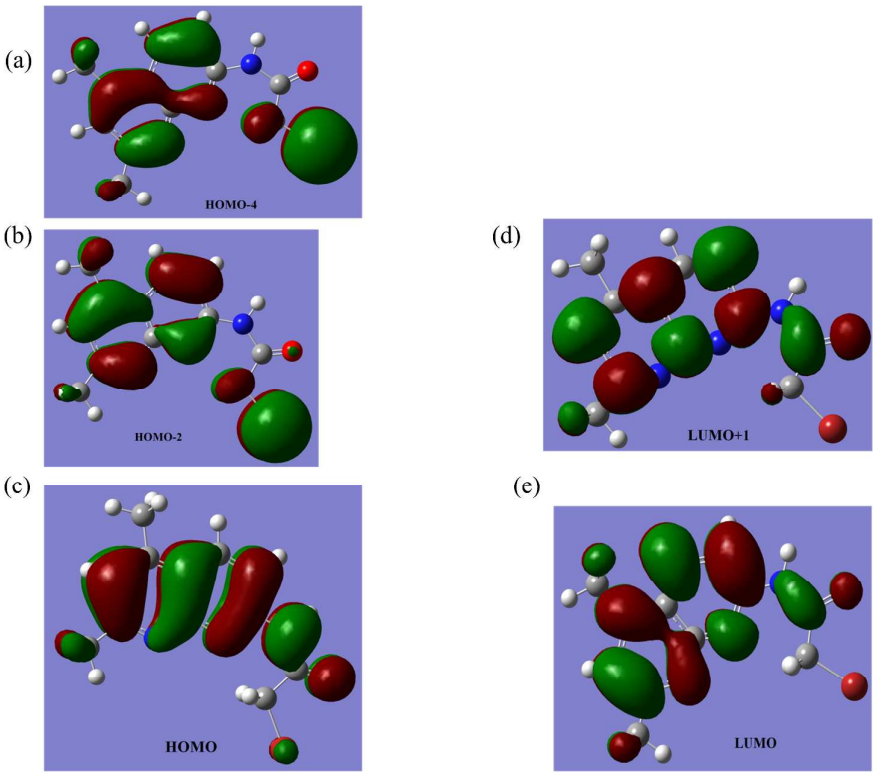

Figure S21. Pictorial view of frontier molecular orbitals of **1a**

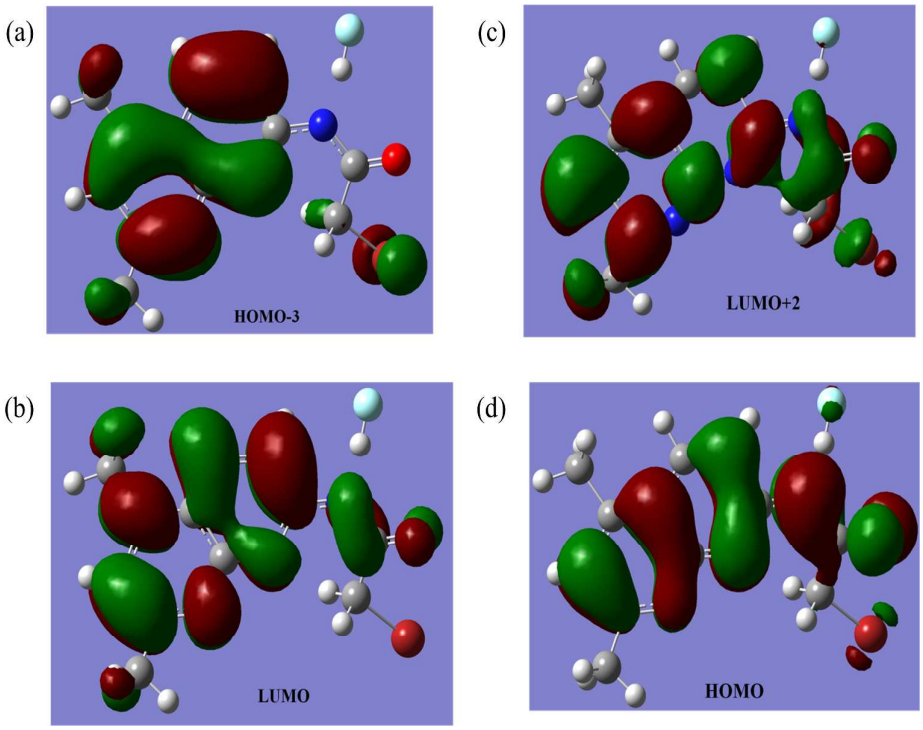

Figure S22. Pictorial view of frontier molecular orbitals of **1a**+F^-.

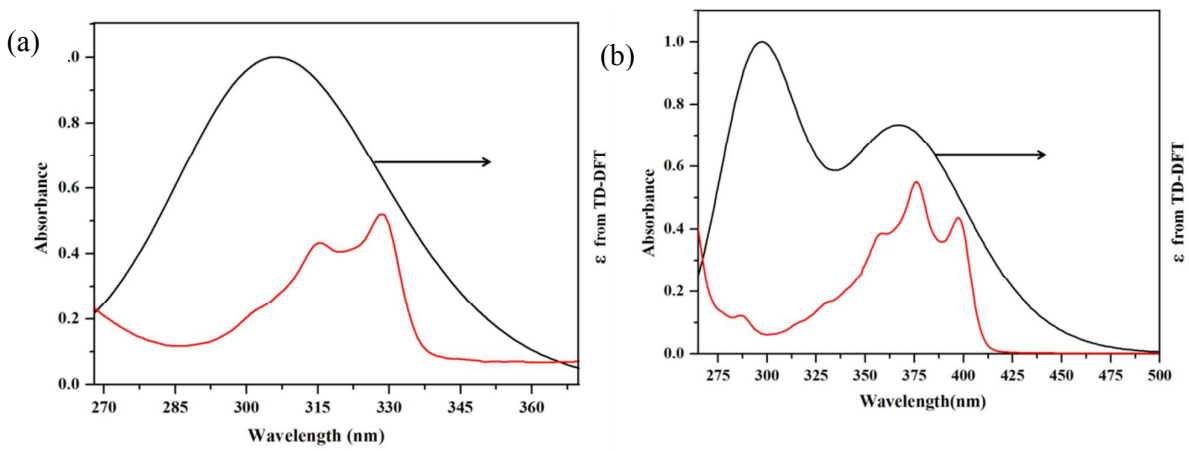

Figure S23. The experimental absorption spectra (a) **1a** (b) **1a**+F^- which were compared with TD-DFT calculated absorption spectral features.

Table S1. Computed vertical excitation wavelength and their orbital contribution using B3LYP/6-311+G(2df,2p).

	λ_{abs}, nm	f[a]	assignment
1a	306.7	0.2089	HOMO → LUMO (90%) HOMO-2→ LUMO+1 (5%) HOMO-4→ LUMO+1 (3%)
	269.5	0.0143	HOMO-2→ LUMO (68%) HOMO→ LUMO+1 (15%) HOMO-4→ LUMO (14%)
1a.F⁻	369.3	0.1926	HOMO→ LUMO (94%) HOMO → LUMO+2 (3%) HOMO-3 → LUMO+2 (2%)
	297.1	0.2588	HOMO→ LUMO+2 (85%) HOMO-3→ LUMO (9%) HOMO→ LUMO (2%)

[a]oscillator strength

Note:

Δλ = 63 nm (Theoretically) for **1a** to **1a**+F^-

Δλ = 69 nm (Experimentally) for **1a** to **1a**+F^-

The electronic spectral data obtained through computational studies are in close agreement with experimental data.

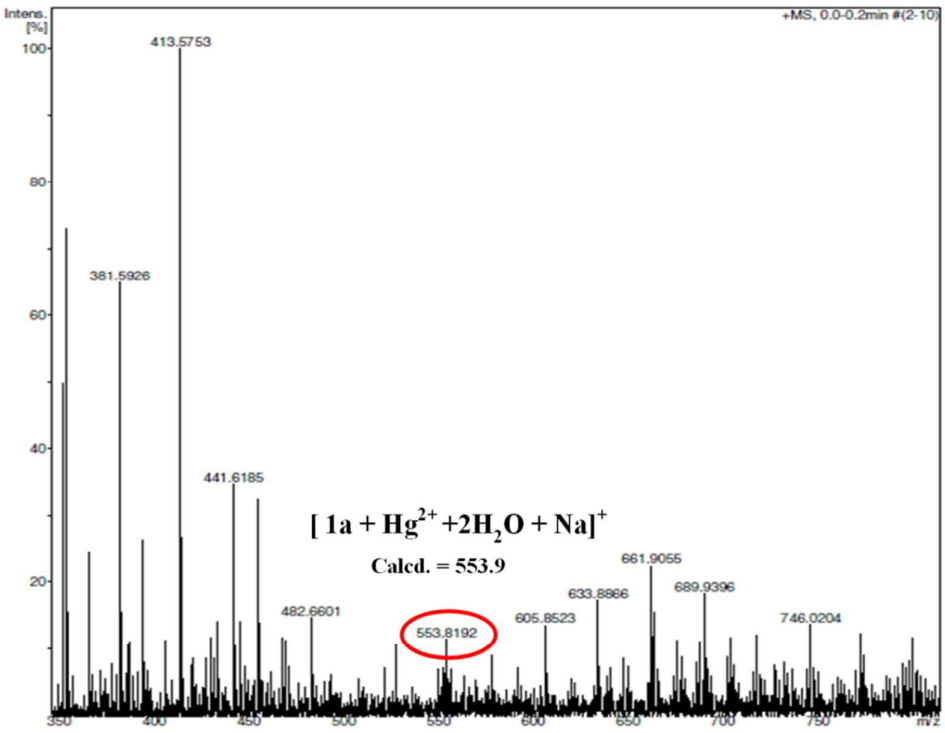

Figure S24. HRMS **(**ESI+) mass spectra of (1:1) complex of **1a** and Hg^{2+} ion.

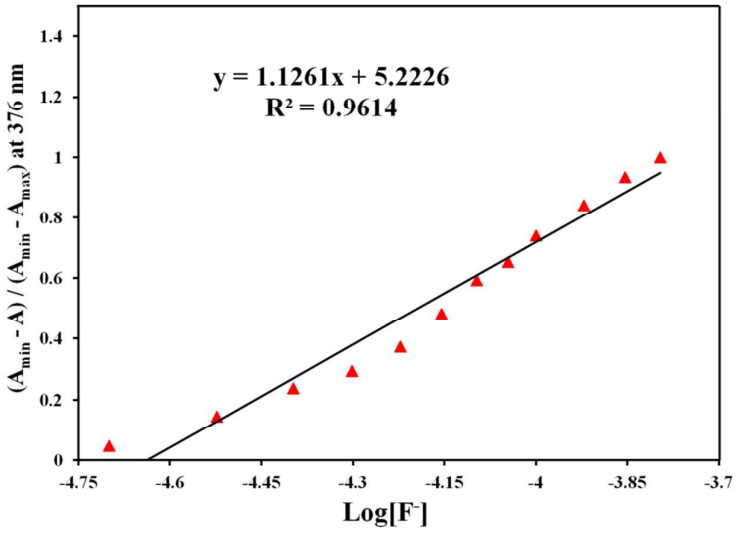

Figure S25. Absorbance of 1a in CH_3CN, normalized between the minimum absorbance was found at zero equiv of F- and the maximum absorbance was found at 4.0 eq. of F^-.

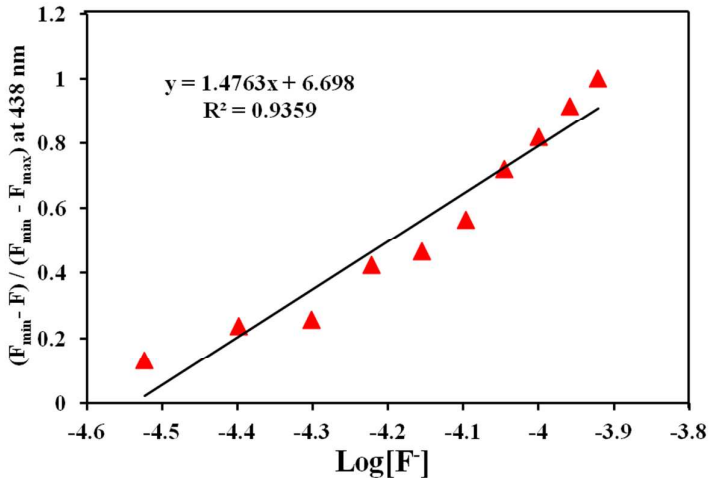

Figure S26. Normalized response of fluorescence signal to changing F^- concentrations for **1a**.

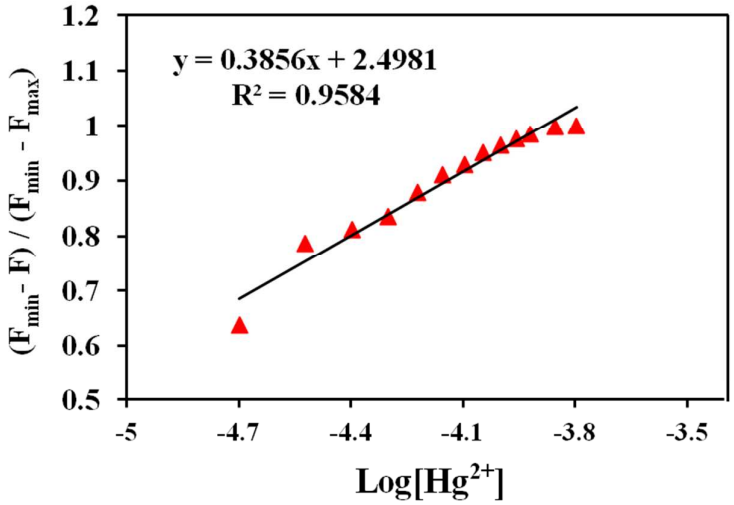

Figure S27. Normlized response of fluorescence signal to changing Hg^{2+} concentrations for **1a**.

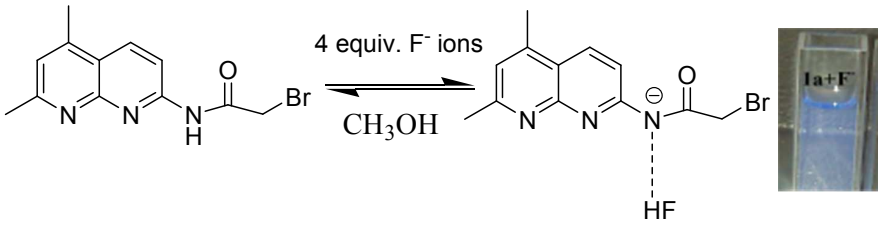

Scheme S1. Schematic representation of binding events while adding 4 equivalents of F^- ions to **1a** and its regeneration upon addition of protic solvents such as methanol.

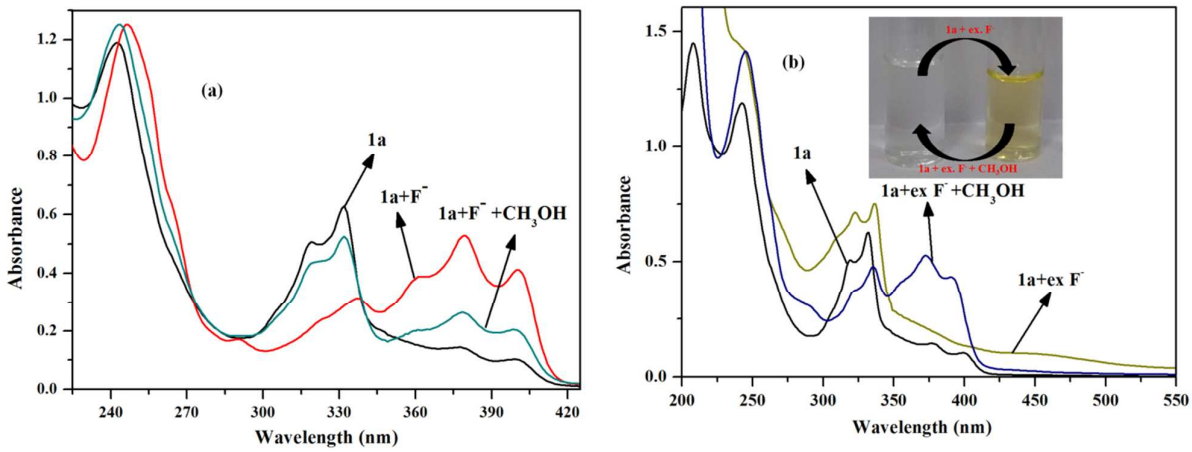

Figure S28. UV-Vis absorption changes (a) after addition of 4 equivalents and (b) excess of F^- ions, respectively with **1a** and its regeneration upon addition of protic solvents such as methanol.

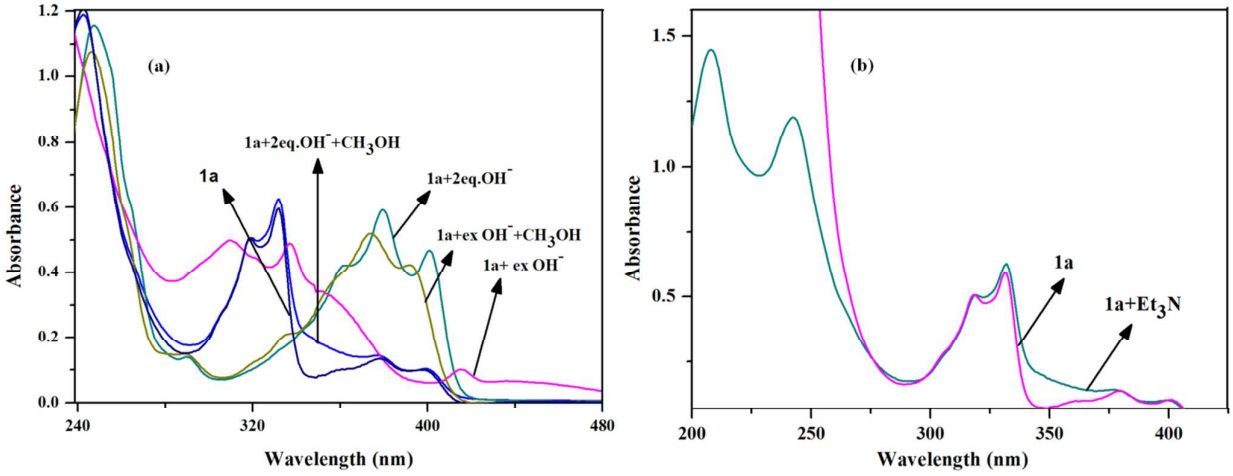

Figure S29. UV-Vis absorption changes (a) after addition TBAOH (b) Et_3N, respectively with **1a**.